UiT The Arctic University of Norway

Faculty of Science and Technology

Department of Physics and Technology

Modelling potential fluctuations due to filaments in the SOL

Elida Veidahl Martinsen

FYS-3907 Master's thesis in Physics and Education - 40 ECTS, June 2024

Abstract

The filtered Poisson process are often used in analysing the fluctuations in the scrape-off layer. This thesis investigates how the FPP-model represents both the ion saturation current, J_{sat} and the velocity signals. The signals are simulated using `blobmodel` [1], with different degree of overlap, for $K = 10^3$, $K = 10^4$ and $K = 10^5$, different amplitudes, set to constant or exponentially distributed, and different distributions of the position in y-direction, degenerated or uniform.

The results show that for the J_{sat} signal, the FPP-model fits well, which also was expected. The results for J_{sat} also showed that varying the distribution for the positions in y-direction, did not affect the results of the model. So for J_{sat}, the FPP-model is a good model for analysing. When analysing the velocity signals, there were more different results. Some of the results show no good analysis of the different signals, but especially for the velocity with exponentially distributed amplitudes, the analysis show also some good results and estimated values. Therefor, the conclusion is that the J_{sat} signal is well represented in the single-point measurement analysis. The velocity signals can also be analysed using the same technique, but does also require some other adaptions, for example include negative values in the analysis.

Acknowledgements

First, I would like to than my supervisor, professor Audun Theodorsen, for good help with all coding issues and lots of guidance through out the thesis. Second, I would like to thank my co-supervisor Gregor Decristoforo, for helping me set up the code for the simulations.

I would also like to thank my fellow students, Heidi and Leni, for many hours in group rooms together, with lots of laughing and some studying. It´s been a hell of a ride.

Lastly, i would like to thank my family, specially my cohabitant, Bendik, for lots of support and always having dinner ready.

Contents

List of Tables

List of Figures

1 Introduction

Fusion energy is one of many research areas with the intention of discovering a clean way to produce energy. This energy form is most known from the stars, where fusion from hydrogen to helium is most common. For the hydrogen to start fusing, it is necessary to have both high temperature and pressure, which requires the fourth aggregate state, plasma. Plasma is heated gas which will results in free ionized particles. Based on these criteria, the fusion on earth are only at a testing state. The research on the fusion energy has already taken place over several years, all the way back to world war two, when the hydrogen bombs become a topic. After this, a lot of theories, and testing has been done. An example is the fusion reactor, tokamak, which has come the farthest in development. The fusion research includes both materials research and plasma research. The main task of doing this research is to extract the net energy from the fusion process.

There are different fusion reactions that are relevant for the fusion energy. For today's research we have the reaction between a deuterium nucleus and tritium nucleus (D-T reaction). This reaction includes tritium, which does not occur naturally on earth due to it's half-life time, but can be extracted from lithium, that is in the earth's crust. However, deuterium is found in the sea water, and are therefore readily available for use in fusion [5]. To contain the plasma in the reactor, the tokamak is shaped like a torus and the plasma is confined by magnetic field lines. This helps maintain the temperature and avoid end loss in the torus. There are many complications in this research, one of them is the fluctuations towards the wall of the reactor, due to the temperature differences between the hot confined plasma and the colder walls of the reactor. Here the plasma forms filaments of hot and dense plasma, also called blobs, which move towards the wall, and potentially damages the reactor.

There is done a lot of research linked to the fluctuations of plasma towards the reactor walls. The research mainly focuses on the blobs, how they are measured and how they propagate. There are several articles describing analysis done on different tokamak, for example TCV [6] and Alcator C-Mod [7]. In addition, there are also done research on both the shape and the propagation of the blobs using numerical simulations, some examples; one focusing on the velocity scaling in SOL [8] and one analysing the amplitude and size of interchange motions [9].

In these articles, they mainly analyse the ion saturation current (J_{sat}) of the fluctuations using filtered Poisson Processes (FPP). The FPP-model takes a superposition of the uncorrelated pulses, K, given in a signal. From before, it is known that the FPP-model gives good results when analysing the ion saturation current signals, but may not work as well when analysing other signal, as velocity. Therefore the main hypothesis for this thesis is to investigate how the single-point measurements captures the density signal well, but not the velocity signal. In this thesis I will use the `blobmodel`, [1], to simulate the 2D structures of the blobs and investigate if the structure is well represented in single-point measurements using the FPP-model.

The thesis is organized as follows. In section 2, the relevant fusion theory are presented, starting with the tokamak, scrape-off layer (SOL), and blob physics, before moving on to the pulse shapes and implementation of these, and then present the Langmuir probe. The stochastic modeling, with necessarily analysing tools, are presented in section 3. Next, a short description of conditional averaging in section 4, before moving on to the experimental setup in section 5. Here the assumption and adoptions to make the simulations, which later are analysed in section6. Start by analysing the ion saturation current, in section 6.1, bu using both the FPP-model and conditional averaging. The same analysis are done for the velocity signals, first for amplitudes set to one in section 6.2, and then for exponentially distributed amplitudes in section 6.3. Finally, the results will be summarised, and a conclusion based on the hypothesis are made in section 7.

1.1 Motivation and school relevance

In the Norwegian school, the subjects are associated with separate curriculum's ("læringsplaner") [10], where the relevant content is presented. This makes it easier for the teacher to decide what to include in the teaching. In the curriculum, there are presented different subcategories, which are core elements ("kjerneelementer") and competence goals ("kompetansemål"). The core elements clarifies the main topics in physics. One of these are energy and energy transfusion. Fusion energy is a topic under this core element, and are therefore a important part of the physics subject. Further in the curriculum, there are presented a lot of different competence goals. There are several competence goals who are relevant to this thesis, which is presented in Norwegian:

- vurdere ulike påstander og argumenter om energi og klima i samfunnsaktuelle problemsstillinger
- forstå begrepet fusjon og vurdere hvordan ulike grunnstoff kan dannes når stjerner lever, kolliderer og dør
- utforske hvordan energi kan gå fra en form til en annen, og vurdere energikvalitet og virkningsgrad i slike overganger
- presentere sentrale elementer i ny viten i fysikk som er et resultat av internasjonalt forskningssamarbeid, og vurdere hvordan slikt samarbeid bidrar i kunnskapsutviklingen
- bruke numeriske metoder og programmering til å utforske og modellere fysiske fenomener
- beskrive elektriske og magnetiske felt og gjøre rede for krefter på objekter med masse og ladning i slike felt

All the competence goals listed above, have some relevance to the main topics of this thesis. Based on the new curriculum's, presented in 2020, both numerically skills and knowledge are important topics. The Norwegian school, has an expectation of competence in these topics. Knowledge I have acquired working with this thesis, gives me a great foundation for the teaching profession, both with the programming and the physical knowledge. Based on these conclusions, this thesis are highly relevant for the teaching professions, especially in physics but also in other topics as mathematics.

2 Fusion basics

In this section, the relevant theory will be presented. I Start by introducing the basic fusion elements as the tokamak, the blob physics, the statistical model and the `blobmodel` used in this project.

2.1 The tokamak

The reactor used to initiate and maintain the fusion reaction is the tokamak. The inside of the tokamak with the most important elements is shown in figure 1. It is shaped like a torus with magnetic field in both poloidal and toroidal direction. The coils, which are used to create the magnetic fields and shape, are placed around the torus both in poloidal, inner and outer, and toroidal direction. This results in both toridal and helical magnetic field, in addition to the plasma electric current [11]. The magnetic field is used to confine the hot plasma inside the reactor. Plasma can be explained as a quasi neutral gas containing free electrons, but also ionized atoms and molecules [12]. The outside of the reactor is called the scrape-off layer (SOL), which are described further in section 2.2 [13].

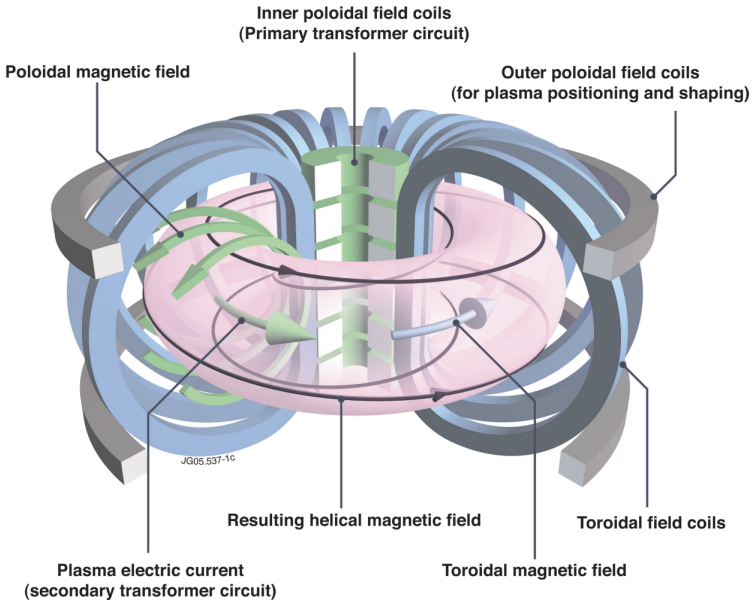

Figure 1: An illustration of the tokamak, which shows how the coils, the magnetic fields and the plasma current is set up in the reactor. Source: EUROfusion [2].

2.2 The Scrape-off layer (SOL)

Some of the most common problems with the fusion reactor is due to the magnetic field and temperature that causes the plasma to fluctuate towards the wall off the reactor. To prevent this movement, there are installed limiters or divertors or both. The limiter is installed on the wall of the reactor, while the divertor is placed at the bottom of the reactor [13]. In figure 2, a cross section of the tokamak is presented. In the middle of the cross section, the confined plasma is located. Here the magnetic field lines is in the plasma. On the figure, it is called the closed magnetic surface, and they do not touch the wall of the reactor or the divertor. Further, the scrape-off layer (SOL) is outside the closed magnetic field lines, where the magnetic field is all the way down to the divertor plates. The limiter structure is placed on the outer wall of the tokamak, and the field lines touching those, is called the wall shadow. The SOL and wall shadow is together representing the open magnetic surface, which are illustrated in the figure 2 [11].

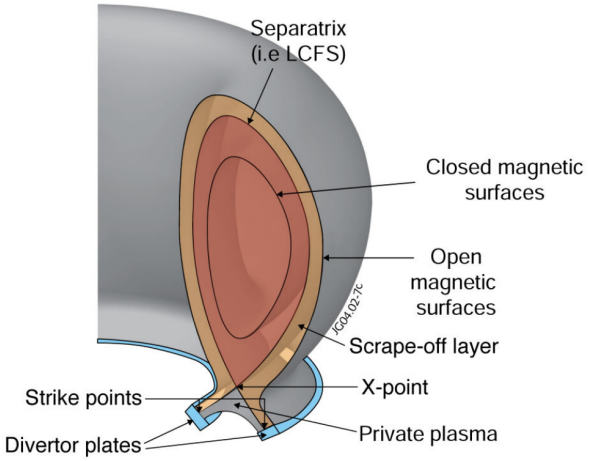

Figure 2: An illustration of the inside of the tokamak. Can clearly see the boundary regions, with a divertor setup. Source: EUROfusion [2].

2.3 The blob physics

In this thesis the main focus lies in looking at the filaments, so called blobs, and how they move. These blobs are a plasma structure that have higher density than the surrounding plasma. Due to their structure, they will move outwards towards the walls of the reactor. The blobs are assumed to be more dense in the middle and less further out [14]. The upset of the isolated blob can be explained using the illustration in figure 3. The figure shows the magnetic field working inwards, which are assumed to be non-uniform. There are also a magnetic curvature gradient working to the left, causing a guiding center drift. The drift are causing the charged particles to separate in the blobs. The negative move to the bottom an the positive to the top, as shown in the illustration. When the charges separate it creates a electric field downwards, which again will cause a $\mathbf{E} \times \mathbf{B}$-drift for the blob, this gives the velocity $u_{\mathbf{E}\times\mathbf{B}}$. The separation of charged particles does also cause a potential and a dipole structure. This structure are also shown in figure 3, where the negative dipole is placed over the negative charges and represented with dotted lines, the positive dipole are around the positive charged, illustrated with straight lines [3].

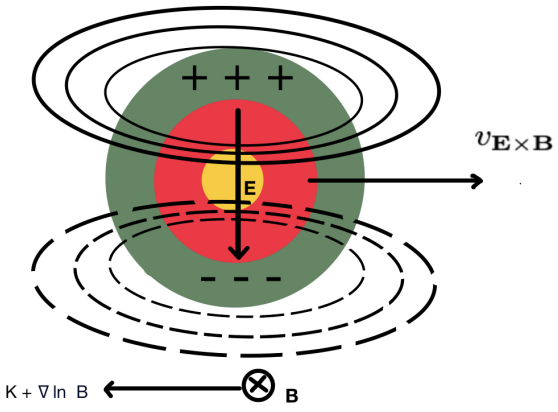

Figure 3: An illustration of the blob, and how the magnetic field, the magnetic curvature and the electric field is causing movement and a dipole structure. The illustration is inspired from the article [3], and also used in a project paper delivered December 2023 [4].

When focusing on one single blob, it is assumed that the different directions will be equal to Cartesian coordinates, locally where the blob is. This means that the coordinates is described by x-radial- , y-poloidal- and z-toroidal direction.

2.3.1 The pulse shapes and velocity

Further, the blobs are described by different pulse shapes in the `blobmodel`, which are described in section 5.1. The main focus will be on the density and the electric potential of the blobs. In the middle of the blob, the density is much higher than further out. Therefore, the density is assumed to be in the middle of the blob in y-direction. The blob will propagate outwards, and it is also known form earlier research that the higher density parts move faster than the parts with lower density [8]. To describe the different signals needed for the analysis, it is necessarily to present different pulse shapes, used in the simulations. Start with the exponential pulse shape in eq. 2.1, which is for $\theta > 0$, and the Gaussian pulse shape presented in eq. 2.2.

$$\varphi_{exp}(\theta) = e^{\theta} \tag{2.1}$$

$$\varphi_{gauss}(\theta) = \frac{1}{\sqrt{2\pi}} e^{-\frac{\theta^2}{2}} \tag{2.2}$$

These two pulse shapes, will represent the simulated ion saturation current signal, with exponential in x-direction and Gaussian in y-direction, as shown in eq. 2.3.

$$\varphi_{Jsat} = [\varphi_{exp}, \varphi_{gauss}] = \left[e^{\theta}, \frac{1}{\sqrt{2\pi}} e^{-\frac{\theta^2}{2}} \right] \tag{2.3}$$

Moving on to the dipole formations on both sides of the high density area. Which is mainly caused by charge separation. Therefor it is also necessarily to present the dipole pulse shape, in eq. 2.4, which together with the Gaussian shape in x-direction will present the electric potential, which is shown in eq. 2.5.

$$\varphi_{dipole}(\theta) = \varphi'_{gauss}(\theta) = -\frac{\theta \cdot e^{-\frac{\theta^2}{2}}}{\sqrt{2\pi}} \tag{2.4}$$

$$\varphi_{Vf} = [\varphi_{gauss}, \varphi_{dipole}] = \left[\frac{1}{\sqrt{2\pi}} e^{-\frac{\theta^2}{2}}, -\frac{\theta \cdot e^{-\frac{\theta^2}{2}}}{\sqrt{2\pi}} \right] \tag{2.5}$$

Further in the analysis of the blobs, the velocity in y-direction is given by the derivative of the dipole pulse shape, eq. 2.4.

$$\varphi_{u_x} = \varphi'_{dipole}(\theta) = \frac{1}{2} e^{-\frac{\theta^2}{2}} \left(\theta^2 - 1 \right) \tag{2.6}$$

$$\varphi_{Uexb} = [\varphi_{gauss}, \varphi_{u_x}] = \left[\frac{1}{\sqrt{2\pi}} e^{-\frac{\theta^2}{2}}, \frac{1}{2} e^{-\frac{\theta^2}{2}} \left(\theta^2 - 1 \right) \right] \tag{2.7}$$

The velocity u_x is given from the $\mathbf{E} \times \mathbf{B}$ velocity $u_{\mathbf{E}\times\mathbf{B}}$:

$$U_{\mathbf{E}x\mathbf{B}} = \frac{\mathbf{E} \times \mathbf{B}}{B^2} = \frac{-\nabla V \times \mathbf{B}}{B^2} = -\frac{1}{B} \begin{bmatrix} -\partial_y V \\ \partial_x V \\ 0 \end{bmatrix} \tag{2.8}$$

from this, the velocity has a pulse shape in both x- and y-direction. Chooses to use the maximum value for the velocity, for simplicity, where the magnetic field are $B = 1$. This gives the velocity in x- direction, u_x:

$$u_x = \frac{\partial}{\partial y} V(x = 0, y)|_{y=0} = \frac{1}{2\sqrt{2\pi}} \tag{2.9}$$

2.3.2 The implementation of dipole pulse shape for this project

The dipole shape given in eq. 2.4 is the first derivative of the Gaussian pulse shape, eq. 2.2. To use the dipole pulse shape in `blobmodel`, it is necessarily to make sure that the dipole pulse shape is normalized by integrating the absolute value and check that it is equal to one. To check this I implement an unknown factor, x, who will show what to multiply the pulse shape with, for it to be normalized. As derived under:

$$\int_{-\infty}^{\infty} x \cdot |\phi(\theta)| d\theta = 1 \tag{2.10}$$

$$\int_{-\infty}^{\infty} x \cdot \left| -\frac{\theta \cdot e^{-\frac{\theta^2}{2}}}{\sqrt{2\pi}} \right| d\theta = 1 \tag{2.11}$$

Which gives an factor $x = \sqrt{\frac{\pi}{2}}$. From this, the normalized dipole pulse shape is given by:

$$\varphi_{Dipole}(\theta) = \sqrt{\frac{\pi}{2}} \cdot -\frac{\theta}{\sqrt{2\pi}} e^{-\frac{\theta^2}{2}} = -\frac{\theta}{2} e^{-\frac{\theta}{2}} \tag{2.12}$$

Then, the normalized signal can be implemented as a new pulse shape in the `blobmodel`. Which further will be used to simulate the floating potential.

2.4 Langmuir probe

Usually the plasma is measured by a Langmuir probe, in the SOL. The probe measures mainly the ion saturation current (J_{sat}), floating potential (V) and the electron temperature. The last one is more difficult to measure, on the timeline for the fluctuations. When analysing the blobs propagating towards the wall, the probe is set up as in the TCV-paper [6]. The probe is shown in figure 4 with J_{sat} measured in the middle and the floating potential, V_{up} on the top and V_{down} at the bottom. Each of these measure points is designed as a Langmuir probe. This means that the probe that is used to measure the blobs consists of three Langmuir probes. In this thesis, the same setup is used when analysing the simulations.

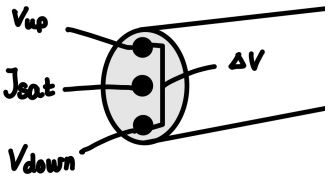

Figure 4: The set up for a Langmuir probe. with the floating potential up, V_{up}, and down, V_{down}, the distance between the floating potential ΔV and the ion saturation current, J_{sat}.

2.4.1 The probe separation

Uses the analytic result for chose the probe separation for the simulations. Want to compare the dipole pulse shape, and the velocity for different distances for the probe separation, dy. Define the dipole pulse shape as φ:

$$\varphi = -\frac{\theta}{2} \cdot e^{-\frac{\theta^2}{2}} \tag{2.13}$$

Further, the dy distance is defined as an array between $0, 1$. The dipole pulse shape to plot for different probe separation dφ is then given by:

$$\mathrm{d}\varphi = \frac{1}{\sqrt{2\pi}} \cdot \frac{\varphi(\mathrm{d}y/2) - \varphi(-\mathrm{d}y/2)}{\mathrm{d}y} \tag{2.14}$$

The velocity U is defined as a constant $U = \frac{0.5}{\sqrt{2\pi}}$.

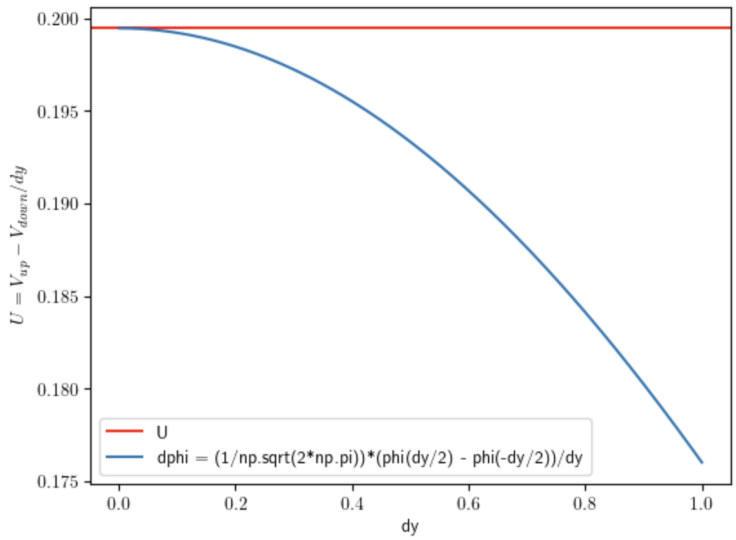

Figure 5: Here the velocity U and the dipole pulse shape *dphi* is plotted for different probe separations dy

The probe separation dy is normalised with the blob size in y-direction. From the plot in figure 5 it is clear to see that the small probe separations is more compatible for the dipole shape than larger once. From this analysis, the probe separation is chosen to be d$y = 0.2$, since it is small enough to be a good separation, but large enough potentially include enough of the area around the J_{sat} measuring point.

3 Stochastic modeling

The stochastic model used to analyse the output of the simulations is called the filtered Poisson process (FPP). This model is commonly used to analyse fluctuations in the scrape-off layer (SOL). The model consist of a superposition of uncorrelated pulses, where the pulses is arranged as a Poisson process. The uncorrelated pulses is described by this model:

$$\Phi(t) = \sum_{k=1}^{K(T)} A_k \varphi\left(\frac{t - t_k}{\tau_k}\right) \tag{3.1}$$

where K is number of pulses, the amplitude is given by A_k, the pulse arrival time is given by t_k, the duration time are given by τ_k and φ is determined by the signal discussed in 2.3.1. When describing the pulses, it is also necessarily to present the intermittency parameter, γ, which describes the degree of overlapping pulses in a time series of pulses. The parameter is given by the ratio between the duration time τ_d of the pulse and the waiting time τ_w:

$$\gamma = \frac{\tau_d}{\tau_w} \tag{3.2}$$

here τ_w is describing the average waiting time for each pulse, and, as mentioned above, the τ_d is the mean duration time for each pulse, which also can be expressed as the mean value of the duration time $\tau_d = \langle t_k \rangle$. From the intermittency parameter, it can be expressed how much overlap of pulses a time series has. For $\gamma \gg 1$, the pulses have much overlap, which means that the shape of the pulse is not easy to see. On the other hand, if $\gamma \ll 1$, the series will have no overlap, and each single pulse can be recognised [15].

Further, from [16], it is necessarily to define the mean value and the variance of the pulses. If the number of pulses K is assumed to be Poisson distributed, then the mean of the pulses can be given by:

$$\langle \Phi \rangle = \frac{\tau_d}{\tau_w} I_1 \langle A \rangle = \gamma I_1 \langle A \rangle \tag{3.3}$$

and the variance is given by the relation

$$\Phi_{rms}^2 = \langle \Phi^2 \rangle - \langle \Phi \rangle^2$$

which also can be expressed as:

$$\Phi_{rms}^2 = \frac{\tau_d}{\tau_w} I_2 \langle A \rangle = \gamma I_2 \langle A \rangle \tag{3.4}$$

From this, the signals can be normalized. Which is necessarily in some cases where the mean value changes over time, an example is the TCV-signal [6]. The normalized signal $\widetilde{\Phi}$ is given by:

$$\widetilde{\Phi} = \frac{\Phi - \langle \Phi \rangle}{\Phi_{rms}} \tag{3.5}$$

The normalization gives out a signal with mean equal to 0 and the variance equal to 1 [17].
The cumulants function is given by [18]:

$$\kappa_n = \frac{1}{\tau_w} \langle \tau A^n I_n \rangle \tag{3.6}$$

which describes stationary independent pulses where the arrival times are from a Poison Process and the pulses are independent of each other. $I_n(\lambda)$ is given by:

$$I_n = \int_{-\infty}^{\infty} [\phi(x)]^n dx \tag{3.7}$$

Then both the mean value and the standard derivation can be found by the characteristic function.

$$\langle \Phi \rangle = \kappa_1 \tag{3.8}$$

$$\Phi_{rms}^2 = \kappa_2 \tag{3.9}$$

It is also relevant to present two other moments, the skewness, S_Φ, and the kurtosis, F_Φ (flatness). The skewness describes the degree of asymmetry to a function, while the kurtosis describes the flatness of the function. These moments can also be expressed by the characteristic function in eq. 3.6, [18]:

$$S_\Phi = \frac{\kappa_3}{\kappa_2^{3/2}} \tag{3.10}$$

$$F_\Phi = 3 + \frac{\kappa_4}{\kappa_2^2} \tag{3.11}$$

For a normal distributed signal, the skewness is $S_\Phi = 0$ and the kurtosis is $F_\Phi = 3$, and for a normalized signal, the skewness and kurtosis are equal [6]. It is also necessarily to introduce excess kurtosis, since that's the result when using the kurtosis numerically. The excess kurtosis is $F_\Phi - 3$.

4 Conditional averaging

In addition to the stochastic modeling, conditional averaging will also be used to analyse the different time series, simulated in this thesis. Conditional averaging finds events in a signal based on different conditions that are given, and then takes the average over the events. It is also possible to do the conditional averaging with a reference signal. Which means that it is possible to look at different times or peaks from the reference signal to the analyse what happens on the new signal at the exalt same point. This way it is easier to see for example what happens in a signal where the reference signal has a peak value [17]. To do the conditional averaging, it is necessarily to find the lower threshold of the signal. The lower threshold used in this thesis is:

$$low_t = 2.5 \cdot \Phi_{rms} + \langle \Phi \rangle \tag{4.1}$$

where ϕ_{rms} is the root mean square value of the signal, which can be found by using the relation in equation 3.4, who describes the variance. Further, the $\langle \phi \rangle$ is the mean of the signal, and are found by using equation 3.3. For normalized signal, with $\langle \phi \rangle = 0$ and $\phi_{rms} = 1$ gives a lower threshold, $low_t = 2.5$.

5 Experimental setup

5.1 The `blobmodel`

The data provided in this thesis is simulated by using the `blobmodel` made by UiT, and can be found here: [1]. For all the simulation, the seed value is held equal. Which means that the pulses is the same for all the different cases simulated.

The model is called `blobmodel`, and simulates the blobs witch are propagating towards the wall of the tokamak. The model does not simulate the physics, but a phenomenological model where the input is blobs with a specific shape, amplitude and velocity. There are four important points to be made; firstly the blobs is intentionally placed with specified time and place. second, the pulses has an specific, constant velocity. Third, the pulses do not interact with each other, but passes right thought each other, and finally, the pulses keeps a constant shape. Further in during the simulations, the focus is on blobs which are moving radially outwards. The simulation do also take the velocity of the blob as the maxima of the pulse velocity of the blob.

5.1.1 Implementation of the model

Start by implementing the dipole pulse shape, eq. 2.4, to the model. To check if the implementations is correctly, the velocity simulated in the program is compared with an analytical value of the velocity. The velocity is simulated by implementing a velocity in x-direction which is not one. The velocity U_{ExB} is given by:

$$U_{ExB} = \frac{V_{up} - V_{down}}{\mathbf{B} \cdot \Delta y} \tag{5.1}$$

where V_{up} and V_{down} is the floating potential up and down measured on the Langmuir probe. Where $\mathbf{B}$ is the magnetic field, which in this case is set to $\mathbf{B} = 1$, and Δy describes the distance between the two probe measurements V_{up} and V_{down}. The analytic value of the velocity is given by:

$$u_x = \frac{1}{2}\frac{1}{\sqrt{2\pi}} \approx 0.19947 \tag{5.2}$$

To control that the simulation is ending with the same value, it is plotted together with U_{ExB}. The velocity U_{ExB} calculated from the simulation of the floating potential given in eq. 5.1, with Δy set to be the difference between floating potential up and down. The velocity is plotted the simulated velocity, from the implementation of the pulse function for velocity eq. 2.6.

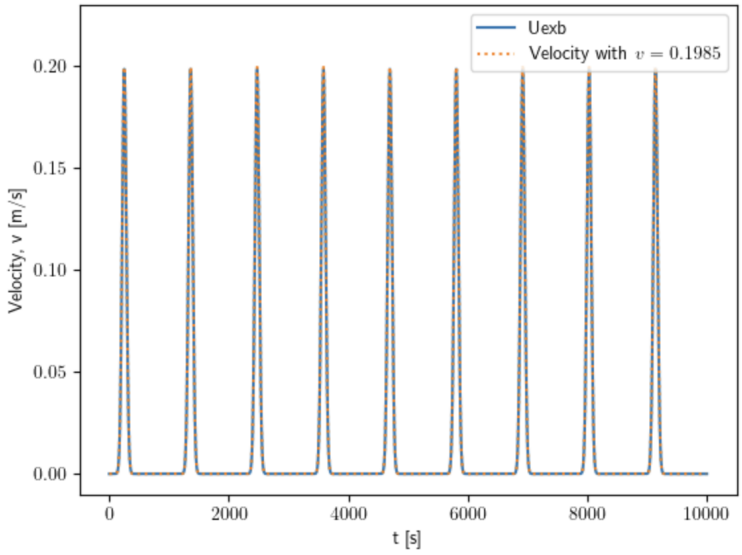

Figure 6: A plot of 10 blobs, equally distributed, with amplitude equal to one.

From the plot in figure 6, the simulation of the velocity and the velocity shape is equal, which means that the simulation is giving the expected velocity for equally distributed blobs, with amplitude equal to one and no overlap.

5.1.2 The time series

Further, to set the experimental setup, three different intermittency parameters is chosen to be analysed, they are $\gamma = 0.1, 1, 10$. To find the correct amount of blobs in a time series with time set to $T = 10000$, the relation for velocity in x-direction is used, given in eq. 2.9 and the intermittency parameter represented in eq. 3.2. To calculate the correct number of blobs, the blob size $l = 1$ and the amplitude $A = 1$

$$\gamma = \frac{\langle \tau \rangle}{\tau_w} = \frac{\langle \tau \rangle \cdot K}{T} = \frac{\frac{1}{u_x} K}{T} = \frac{2\sqrt{2\pi} \cdot K}{T} \tag{5.3}$$

$$K = \frac{\gamma \cdot T}{2\sqrt{2\pi}} \tag{5.4}$$

It is important to simulate a time series, long enough to only show the stationary signal. If the time series is to short and the intermittency parameter is high, the signal will start with a transient and then have the stationary signal, which is whats analysed. The transient will effect the analysis, and it is therefore important to check that the series is long enough. An example of this is shown in figure 7.

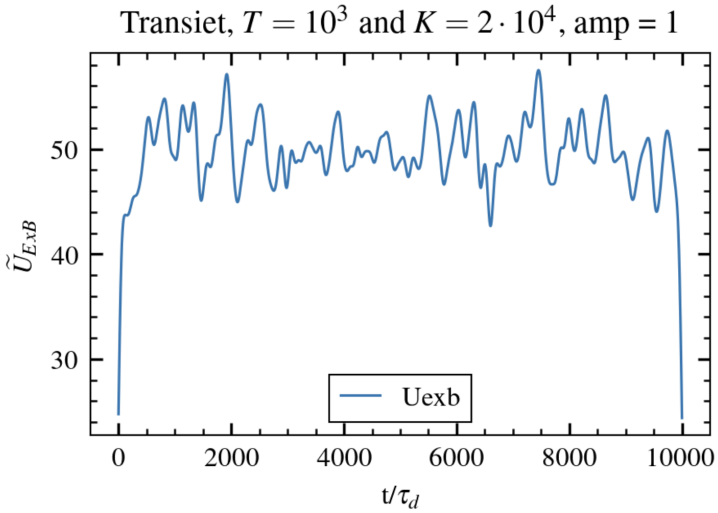

Figure 7: A signal with $T = 1000$, where the transient is clearly showing (from 0)

Therefore the time of the signal is chosen to be $T = 50000$. Then, by using eq. 5.4, the number of blobs that are necessarily for the intermittency parameter γ is easily found. The number of blobs is constant for the different cases. These values are shown in the table 1.

Table 1: The calculated number of blobs needed for the belonging intermittency parameter γ.

γ	K
0.1	$\approx 10^3$
1	$\approx 10^4$
10	$\approx 10^5$

6 Results and discussion

In this section, the results will be presented and discussed. It will cover three different cases, which are different due to different degree of overlap. This means that the time series has a constant time, but different number of blobs in the three cases. These cases will be analysed by looking at different amplitudes and position in y-direction. When the position in y-direction is set to be uniformly distributed, the interval is set to $[0, 3Ly]$, to be sure that the distribution is covering all the values for the signal. The analysing will be done by using the FPP-model and conditional averaging.

6.1 Results of the density signal Jsat

Here comes an analysis of the density signal J_{sat}, where it is expected good results since the FPP-model works good for experimental data. In this section, statistical models will be shown and analysed for the ion saturation current, J_{sat}. There are simulated different cases for the ion saturation current, to see how the FPP-model works for both different degree of overlap, different amplitudes and different position in y-direction. The ion saturation current are simulated using first amplitude set to one and then amplitude set to be exponentially distributed. The position in y-direction is also set to be degenerated distributed, and uniformly distributed. The different degree of overlap are divided into number of blobs $K = 10^3, 10^4, 10^5$. Further there are two different amplitudes used, the amplitude are set to one for the different degree of overlap, and then set to exponentially distributed for the same cases with overlap. The position in y-direction is also changed for all the different cases above, first set to be degenerated distributed, and then set to be uniformly distributed. In figure 8 and 9, the relevant time series are normalized, by using eq. 3.5, and presents $\widetilde{J}_{sat}$. These will be further analysed to confirm that the `blobmodel` is a good approximation, for analysing the signal. To show how the pulse shape is looking, and the degree of overlap, it is chosen to plot the time series in the time interval $[0, 10^4]$.

In figure 8, the time series with amplitude set to one is shown. The series with same number of blobs (K) is set besides each other to compere how the position in y-direction effects the pulses. For the first case with $K = 10^3$, the pulses has little overlap, which means that they are mostly separated. One of the differences when changing the position in y-direction is amplitudes of the pulses. For a degenerated distributed y-position, the pulses have even amplitudes, but for the uniform distributed y-position the pulses has much smaller amplitudes, and also variate more. For larger degree of overlap, $K = 10^4$ and $K = 10^5$, the differences are harder to see.

Further, in figure 9, the different time series with amplitude set to be exponentially distributed. For these time series the velocities are different for each pulse, which also causes different duration time for the pulses. This comes clear in the plots with $K = 10^3$, where the pulses are unlike each other. For the other cases with $K = 10^4$ and $K = 10^5$, the pulse shapes and the duration times for the pulses are more difficult to see.

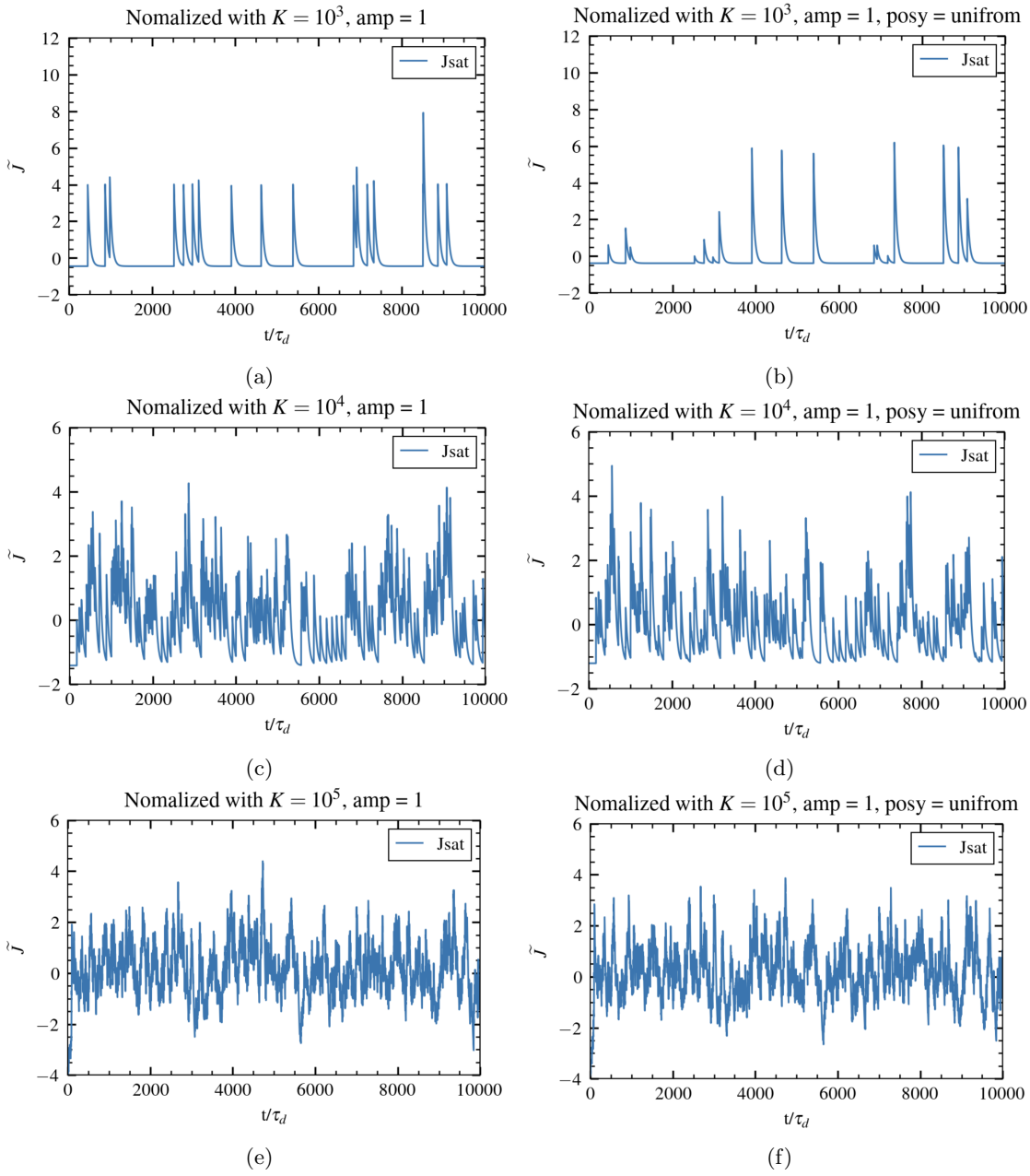

Figure 8: The time series for the normalized ion saturation current J_{sat}, with amplitude set to one. To the left, the time series with degenerated distributed position in y-direction is presented, and to the right the position in y-direction is set to be uniformly distributed.

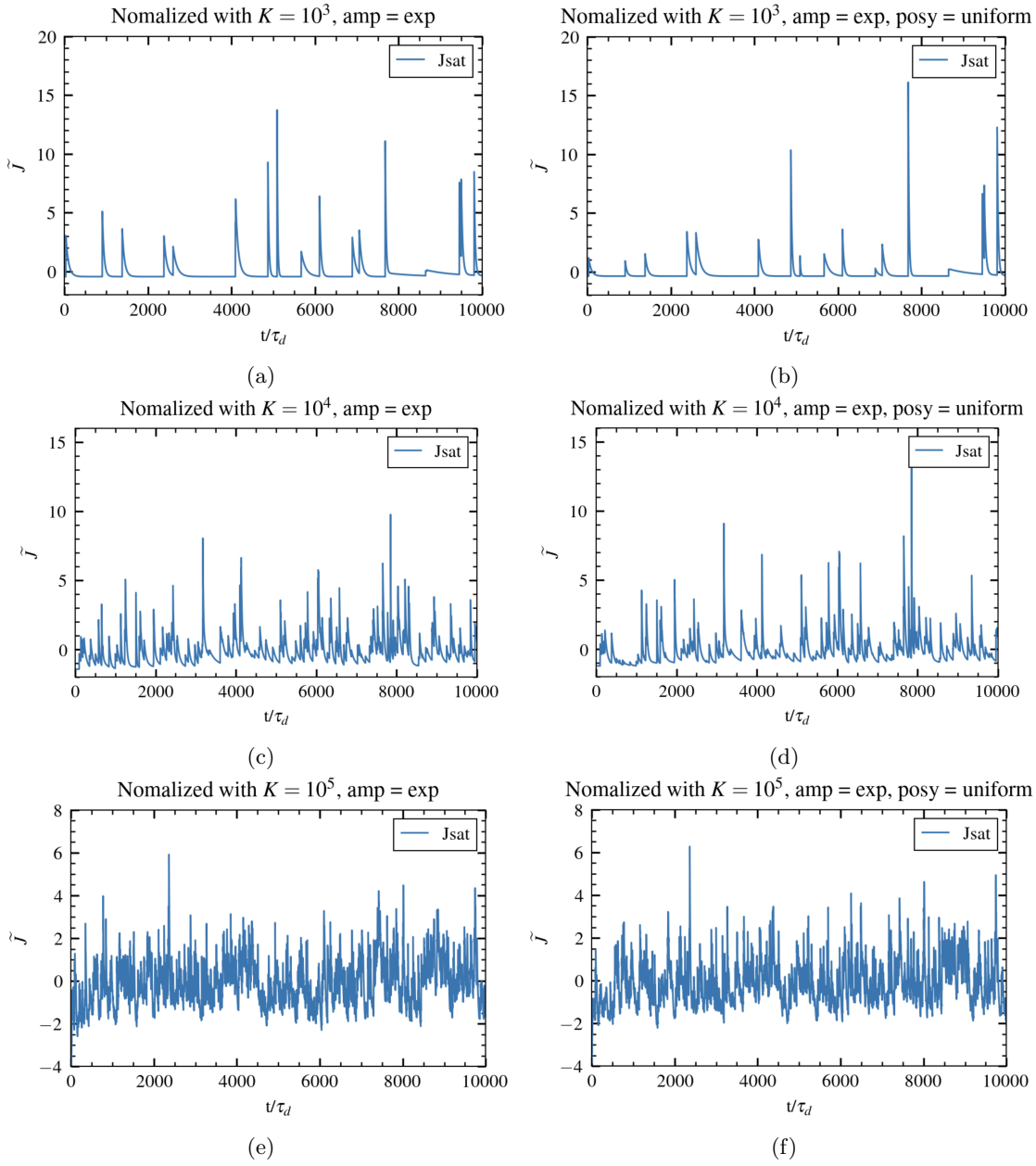

Figure 9: The time series for the normalized ion saturation current J_{sat}, with amplitude set to be exponentially distributed. To the left, the time series with degenerated distributed position in y-direction is presented, and to the right the position in y-direction is set to be uniformly distributed.

In the FPP-model, the analysing method is using a gamma distribution to see the theoretical shapes. Which can be used to compere the simulated results with. Since half of the data is set with amplitude equal to one, it means that the fit may not be as good as an estimate. Therefor, it is necessarily to also look at the different momentum values.

The skewness and flatness are calculated numerically, directly from the normalized time series, and presented in table 3 and 4. The skewness and flatness can also be calculated analytic by using the equations presented in section 3. The calculations are done for the cases with amplitude set to one, where the waiting time τ_w is given by:

$$\tau_w = \frac{T}{K} \tag{6.1}$$

where T is the length of the time series, and are set to $T = 50000$ for all cases. The number of blobs K is defined as $K = 10^3$, $K = 10^4$ and $K = 10^5$ for the different cases. This gives the waiting times $\tau_w = 50, 5, 0.5$. This can be used further to calculate the different cumulant function

given in eq. 3.6. The mean duration time τ_d is a constant when the amplitude is set to one, and are the given by:

$$\tau_d = \frac{l}{u_x} \tag{6.2}$$

where l is the size of the blob and set to $l = 1$, and u_x is the velocity and are determined from eq. 2.9. With $A = 1$, this gives $\tau_d = 2\sqrt{2\pi}$. For the J_{sat} signal, the integral of the pulse function are given as $I_n = 1/n$. To calculate the theoretical skewness and excess flatness, the equations given in eq. 3.10 and $F_\Phi - 3$ where the kurtosis, F_Φ is given in eq. 3.11. The analytic values are presented in table 2.

Table 2: The skewness, S_Φ and flatness F_Φ for the different cases, calculated analytic.

Jsat, amp = 1	K = 10^3	K = 10^4	K = 10^5
S_Φ	2.9775	0.9416	0.2977
$F_\Phi - 3$	9.9736	0.9974	0.0997

For amplitude set to one, the skewness is nearly what's expected, but the excess kurtosis is more varying. Compared with the numerical values for skewness, the case with amplitude set to one and degenerated distributed position in y-direction is the most equal case, where there are only small differences. Moving to the other case with amplitude set to one and uniform distributed position in y-direction, the skewness are still equal to the analytic values, but the differences are larger than for the first case. When looking at the cases exponential distributed amplitudes there are a more significant difference. For the case with degenerated distributed position in y-direction, the values is approximately double the value for amplitude set to one. Which means that asymmetry is larger for the exponential distributed amplitudes, which corresponds with the differences in the pulses, which is discussed above.

Moving on to excess kurtosis, the differences for all the signals are larger. Starting with amplitude set to one, the difference are small when the number of blobs are set to $K = 10^3$ and gets larger when the number of blobs increases. Looking at the exponentially distributed amplitudes, the differences are even larger.

However, there are a common trend for all the different cases. When the number of blobs increases, the skewness and kurtosis both decreases. This means that the signals get more symmetric with higher degree of overlap. Both the skewness and the excess kurtosis are higher when the the position is uniformly distributed. Which means that when the position no longer are degenerated distributed, the signals are more asymmetric and has less flatness.

Table 3: The skewness, S_Φ and excess kurtosis $F_\Phi - 3$ for the different cases, found numerically from the simulated signals. For J_{sat} with amplitude set to one.

amp = 1	K = 10^3	K = 10^4	K = 10^5
S_Φ	3.023	0.934	0.287
$F_\Phi - 3$	10.570	1.002	0.097
amp = 1, posy	K = 10^3	K = 10^4	K = 10^5
S_Φ	3.084	1.212	0.365
$F_\Phi - 3$	16.480	1.684	0.143

Table 4: The skewness, S_Φ and excess kurtosis $F_\Phi - 3$ for the different cases, found numerically from the simulated signals. For J_{sat} with exponentially distributed amplitude.

amp = exp	K = 10^3	K = 10^4	K = 10^5
S_Φ	6.054	1.912	0.591
$F_\Phi - 3$	61.248	6.418	0.586
amp = exp, posy	K = 10^3	K = 10^4	K = 10^5
S_Φ	7.771	2.518	0.794
$F_\Phi - 3$	99.995	11.276	1.112

6.1.1 Probability density function, PDF

In figure 10, the J_{sat}-signal with amplitude set to one, is shown. For the first case, representing $K = 10^3$ in green, it is a change in the plot around $\widetilde{J} = 4$ in figure 10a and around $\widetilde{J} = 6$ in figure 10b. The reason for these are that the individually pulses is registered first and after these, the pulses who have some overlap is presented in the PDF. These values for the normalized J_{sat}-signal can be confirmed by looking at the time series in figure 8a and 8b, where it is easy to see that the singular pulses reaches the values where the change are, $\widetilde{J} = 4$ for figure 8a and $\widetilde{J} = 6$ for figure 8b. For both case two ($K = 10^4$) and case three ($K = 10^5$), the functions are more equal to whats expected. Based on the estimated intermittency parameter, the case with amplitude set to one, are more equal the Gaussian function. From the figure it is also clear that for higher overlap the probability density higher for lower values of $\widetilde{J}_{sat}$, which indicates that the signal is denser for lower values, which also can be seen in the time series in figure 8. Overall, the probability density function gives no impression that the position in y-direction affects the function. Further, the estimated intermittency parameter, γ, is given in the figure 10. These γ-values, gives that case one has little overlap ($\gamma \approx 0.64, 0.66$), case two has some overlap ($\gamma \approx 4.9, 2.9$), and case three has much overlap ($\gamma \approx 61, 31$).

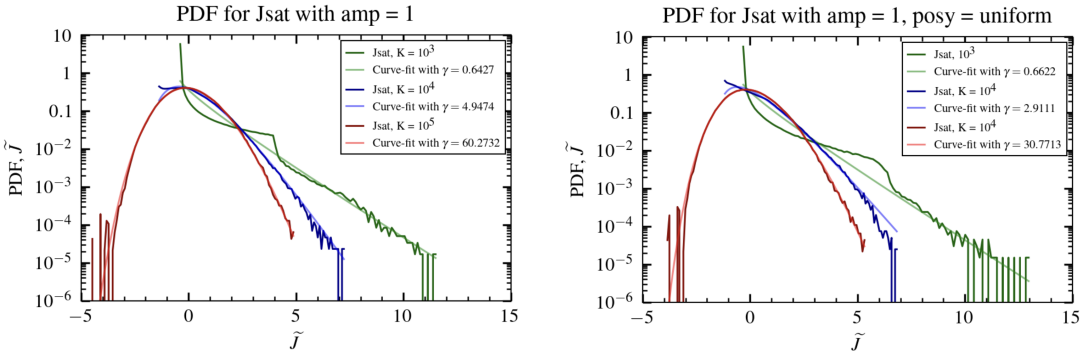

(a) (b)

Figure 10: The probability density function for the ion saturation current, with different number of blobs. The amplitude set to be one.

The same analysis is done for the cases, where the amplitude is set to be exponentially distributed, shown in figure 11. The PDF for $K = 10^3$, is more evenly distributed compared to when the amplitude is set to one. The other two cases looks more like an Gaussian function, which indicates that the model fits good for these cases. This can also be seen, looking at the different estimated intermittency parameters. Looking at figure 11a, the estimated intermittency parameter is given as $\gamma \approx 0.1, 0.9, 10.5$, which is nearly equal to whats expected for the three different cases. For figure 11b, where the position in y-direction is set to be uniformly distributed, the intermittency parameter is estimated to $\gamma \approx 0.06, 0.56, 5.7$. These values are almost half of whats expected. This means that the position affects the PDF's, based on whats shown in the estimated intermittency parameters. Further, it is possible to see that for small values off the ion saturation current, the probability density is around the same values, but for larger ion saturation current, the the probability density is more different. There are higher values for the current, when the degree of overlap is lower.

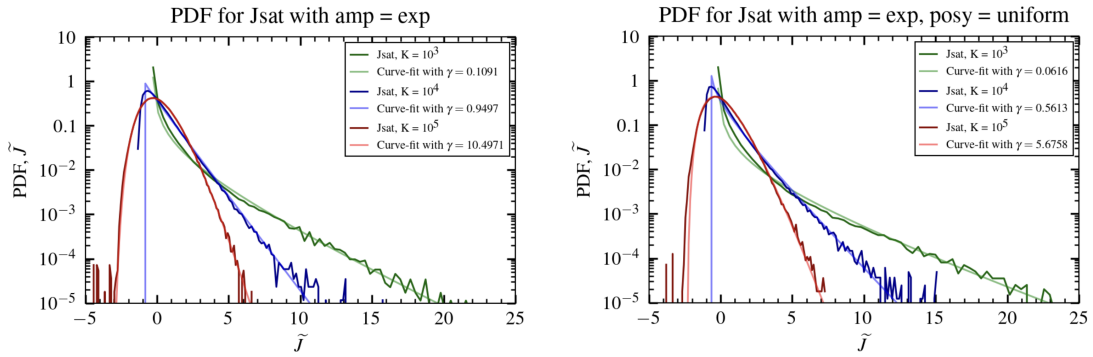

(a) (b)

Figure 11: The probability density function for the ion saturation current, with different number of blobs. The amplitude set to be exponentially distributed.

6.1.2 Power spectral density function, PSD

The power spectral density function is showing the relation between the frequency and the amount of energy in the signal. Compared to other analysis done on the ion saturation currents, the PSD is as expected. In figure 12a and 13a, the different PSD functions for the given time series are presented. The lower frequencies has the highest amount of energy. Here the function is flat for smaller frequencies, and has a even decay when the frequency reaches $\approx 10^{-2}$. The PSD functions are independent of the number of blobs, K, and therefore has equal shape for each plot. This can also be confirmed by looking at the different duration time τ_d given by the estimated curves in figure 12a and 12b. The duration time is both $\tau_d \approx 8$. See that for the two different amplitudes, the functions are similar. There are some small differences between the different amplitude. It is easy to see by looking at the point where the PSD function crosses frequency $= 0.1$. See that the figure 12, with amplitude set to one has a lower power at $freq = 0.1$. While, in figure 13, the power has a higher value for the same point $freq = 0.1$. As mentioned for amplitude set to one, the exponentially distributed amplitudes does not affect the dependency of K, in figure 13a and 13b the duration time $\tau_d \approx 6$, which are equal each other, but slightly different from the first PSD plots.

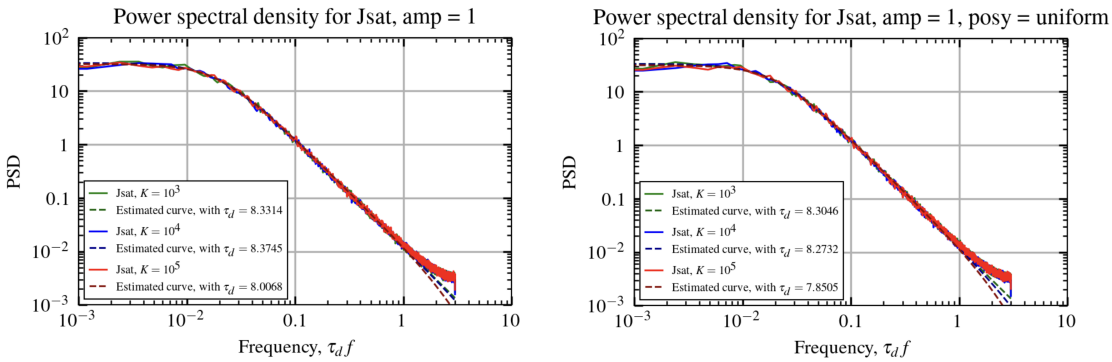

(a) (b)

Figure 12: The power spectral density for the ion saturation current with amplitude set to one.

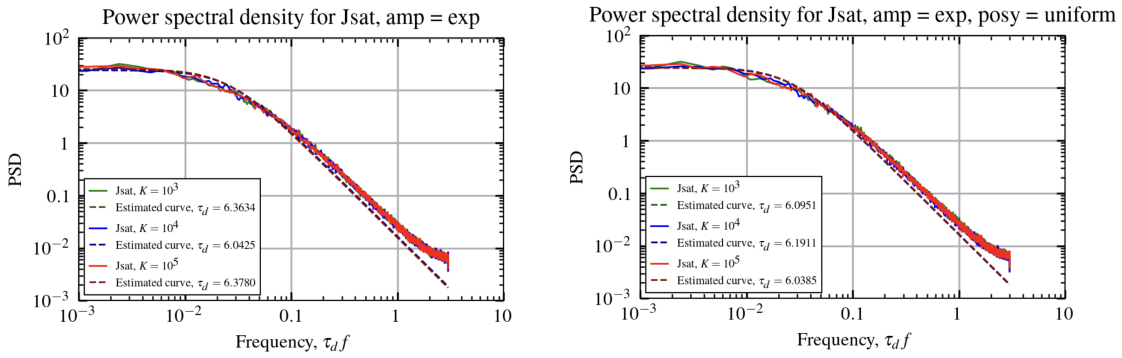

(a) (b)

Figure 13: The power spectral density for the ion saturation current with amplitude set to be exponentially distributed.

6.1.3 Conditional averaging

The conditional averaging is to analyse different average of the pulses. Here it is interesting to look at the average pulse shape, amplitude distribution and the waiting time distribution (τ_w). To do this analysis, it is necessary to find a lower threshold, to pick the relevant pulses to do the conditional average over. This lower threshold i chosen to be the standard value given by eq. 4.1. Since the signal is normalized, which gives $mean = 0$ and $std = 1$, the lower threshold are $low_t = 2.5$. Look at the time series in figure 8 and 9 to control which pulses that are included in the conditional averaging. See that there are some variety in which pulses are included in the cognitional average, for the case with $K = 10^3$, some of the smaller pulses are also included, but for higher K, the smaller pulses are avoided when doing the conditional average. This means that the analysis are done mostly on the overlapping pulses, and the singular pulses are less represented. This will not affect the analysis, but it is important to be aware of when interpreting the results.

In figure 14, the average pulse shape for the three different cases, where the amplitude is set to one, is presented. The expected pulse shape is easy to see form the time series plot (figure 8 and 9) with the lowest number of blobs $K = 10^3$. It is also shown in the figures for pulse shape, in case one with little overlap, blue pulse shape in the figures. For these different cases it is easy to see that the raise of the pulses are very different, while the decay is almost identical.

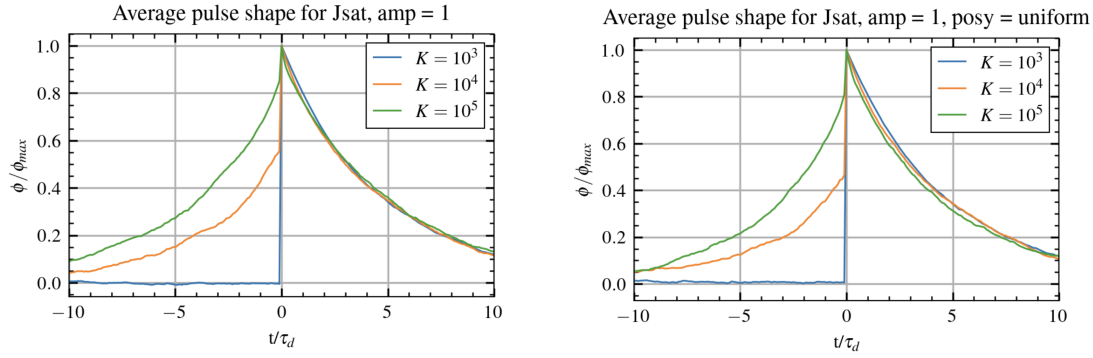

(a) (b)

Figure 14: The average pulse shape for the three different cases, with amplitude set to one.

In figure 15, the same analysis is done but for the signals with exponentially distributed amplitudes. In these figures, the rise time is also more unlike than the decay time. However, they are all more like each other, and the differences are smaller when the signal has exponentially distributed amplitude. In these plots it is also shown that when the position in y-direction is uniformly distributed, the differences are smaller than when the position is set to be degenerated distributed. The expected shape for the ion saturation current is a exponential pulse shape, which is exactly

whats shown in the different plots. The degree of overlap effects the raise of the exponential shape, but do not effect the exponentially decay in large degree.

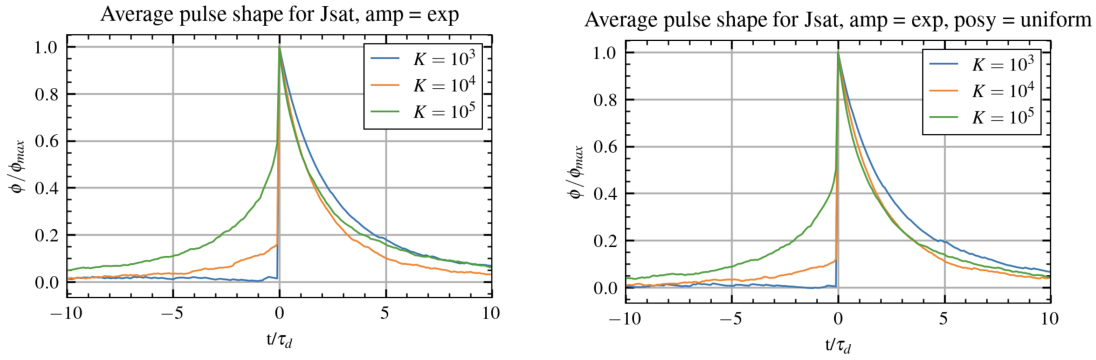

(a) (b)

Figure 15: The average pulse shape for the three different cases, with exponentially distributed amplitude

Remembering form earlier that the waiting time is calculated from number of blobs K and the length of the time series $T = 50000$, which gives the waiting times for the different cases, $\tau_w = T/K = 50, 5, 0.5$. It is important to remember that this is for the all the pulses in the time series. By looking at the belonging time series in figure 8, and knowing that the lower threshold is set to 2.5. The waiting times for the first case, when $K = 10^3$, should be similar to the theoretical values, since most of the pulses are included. For the other cases, there are less pulses included, which means that the waiting time are higher than whats expected. In figure 16 and 17, the different waiting time distributions are presented, with the estimated waiting time. Start by looking at the waiting time distributions for amplitudes set to one in figure 16. In these plots, both the distributions and the estimated curve-fits, are quite equal to each other. Which indicates that the waiting time is also similar to each other. For the case with $K = 10^3$, and degenerated distributed position, the waiting time is nearly as expected. For all the other cases, the estimated values are higher than the theoretical values, which is also expected, and confirms that the lower threshold avoids many of the smaller pulses in the signal, which will give higher waiting time between each pulse.

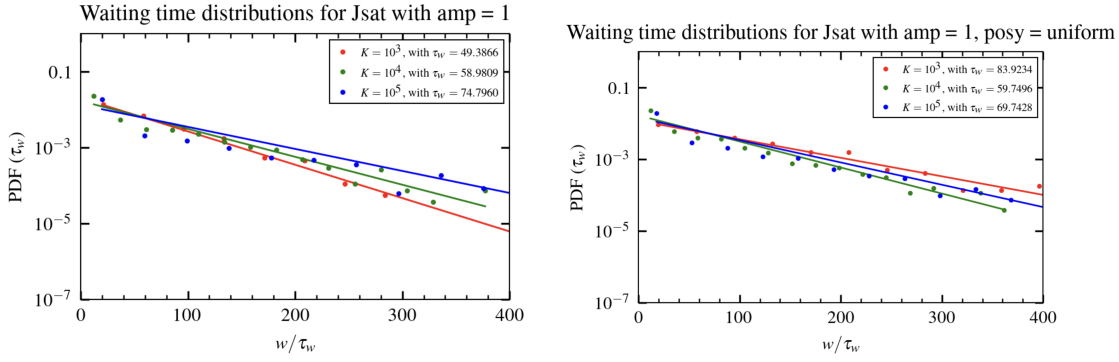

(a) (b)

Figure 16: The waiting time distribution for the ion saturation current signal with amplitude set to one.

In figure 17, the same analysis is presented for the exponentially distributed amplitudes. Compared to the first cases with amplitude set to one, there are larger differences between the different cases. Given the theoretical waiting times, it is easy to see that there are clearly differences to the numerically values. For the different cases with $K = 10^3$, the waiting time is much higher than expected. Looking back at the time series in figure 9, the lower threshold exclude more pulses also for the lower K. This is also easy to see in the estimated waiting time values in the plots for

$K = 10^3$, where the values are nearly double of the theoretical values. For the other two cases, $K = 10^4$ and $K = 10^5$, the estimated values are lower than for the cases with $A = 1$.

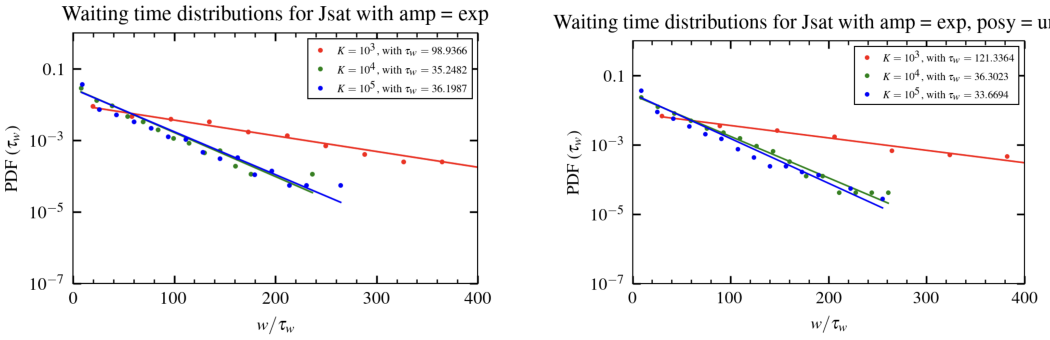

(a) (b)

Figure 17: The waiting time distribution for the ion saturation current signal with exponentially distributed amplitudes.

Further, the conditional averaging are used to look at the amplitude distributions for the different cases, which are presented in figure 18 and 19. These function shows the probability density for different amplitudes. Start by looking at the case for amplitudes set to one, presented in figure 18. The case with $K = 10^3$, in red, shows small sign of being exponentially distributed, but the fit are not perfect. See the highest point in both the left and right plot, which represents all the singular pulses, $A \approx 4$ and $A \approx 6$. This is the same values as discussed for the probability density function in section 6.1.1. For the two other cases with $K = 10^4$ and $K = 10^5$, the distributions show that the connection with the amplitudes are some exponentially distributed, even though the individual amplitudes are equal. This may therefore be caused by the overlap, and results in different amplitudes in the time series.

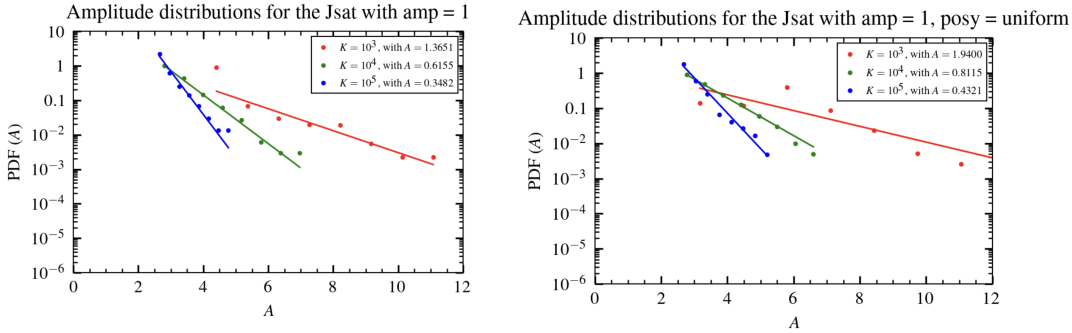

(a) (b)

Figure 18: The amplitude distribution for the ion saturation current signal with amplitude set to one.

The amplitude distribution to the exponential distributed amplitude cases are presented in figure 19. See some similarity to the case with amplitude set to one. However, for higher number of blobs the amplitude distributed are well presented with a exponential distributed fit function. There are also done similar discoveries in [17], where he discuss the effect of the intermittency parameter in amplitude distributions.

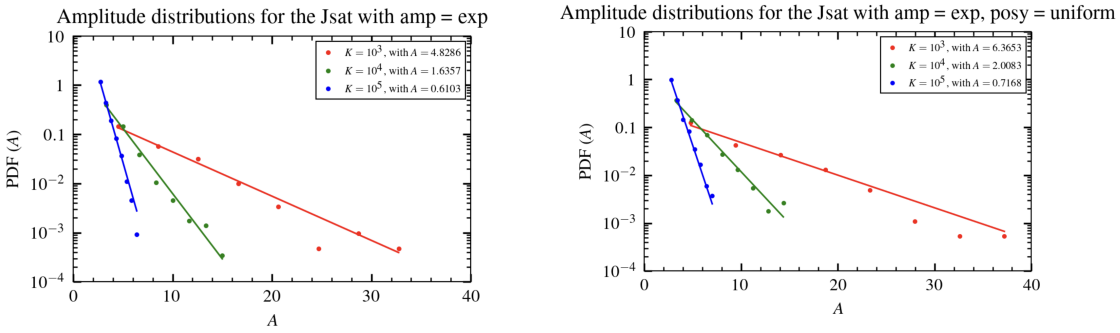

(a) (b)

Figure 19: The amplitude distribution for the ion saturation current signal with exponentially distributed amplitudes.

6.1.4 Summary of finds in analysing the ion saturation current signal

When analysing the ion saturation current using both the FPP-model and conditional averaging, the result are as expected. Started by looking at the skewness and excess kurtosis, where it is confirmed that the theoretical and numerical distributed moments are similar for the cases with amplitude equal to one. For the exponentially distributed amplitude cases, the moments where different from the theoretical, which is also expected since the theoretical values are calculated for amplitude set to one. Moving on to the FPP-analysis, where both probability density functions and Power spectral density present the signals as expected. For the PDF, the exponentially distributed amplitude cases, give surprisingly good estimates for the intermittency parameter γ. For PSD, the functions showed expected values with equal PSD for the different cases, so independent of K. When changing the position to be uniformly distributed, the model still is presenting the signals good both for PDF and PSD, which shows how robust the model is. Moving on to the conditional averaging, the results confirms the information's presented in the FPP-analysis, with the pulse shapes, waiting time distributions and amplitude distributions. This section confirms therefore the first part of the main hypothesis.

6.2 Results of the velocity signal with amplitude set to one.

Moving on to the velocity analysis, starting with the cases with amplitude set to one, and analysing this the same way as done for the ion saturation current signal in section 6.1. In figure 20, the relevant time series are presented with amplitude set to one. On the left side the y-position is set degenerated distributed and on the right side it is uniformly distributed.

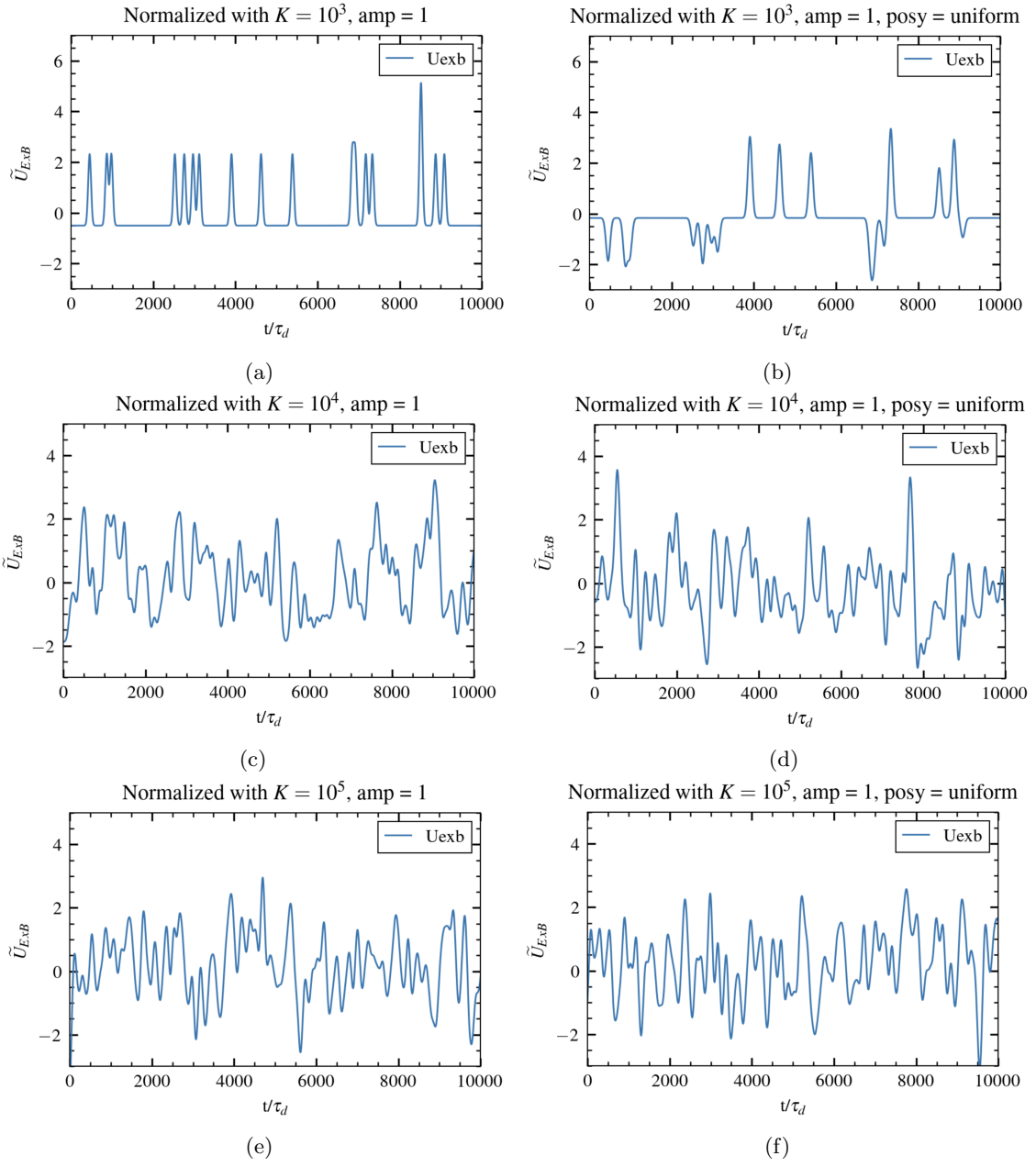

Figure 20: Plots of velocities for different intermittency parameter who are equally distributed blobs with amplitude equal to one. To the left the position in y-direction is set to be degenerated distributed, and to the right the position in y-direction is uniformly distributed.

Start by looking at the case with $K = 10^3$, where the pulses are evenly spread with little overlapping pulses. One clear difference due to the position in y-direction is the direction of the pulses. For the degenerated distributed position in y-direction, the pulses only have positive pulses, but for the uniform distributed position the pulses are both positive and negative. This is probably due to the measuring points on the blobs. For the degenerated distributed position, there are only measured positive pulses. When the position are set to uniformly distributed, the measuring point may also reach the negative parts of the blob shape. For both cases with $K = 10^4$ and $K = 10^5$,

there are more difficult to see the separated pulses due to more overlap. Due to the overlapping pulses there are also more difficult to see the difference in the pulses due to the position.

In table 5, the skewness and excess kurtosis are calculated analytic, with the integral of the pulse function given by:

$$I_n = \frac{(2\pi)^{\frac{1}{2}-\frac{n}{2}}}{\sqrt{n}} \tag{6.3}$$

Set this into the cumulant function, presented in eq. 3.6, along with the duration time $\tau_d = 2\sqrt{2\pi}$ and waiting time $\tau_w = 50, 5, 0.5$. Put this into the equations given for skewness 3.10 and kurtosis 3.11.

Table 5: The skewness, S_Φ and excess kurtosis $F_\Phi - 3$ for the different cases, calculated analytic.

Uexb, amp = 1	K = 10^3	K = 10^4	K = 10^5
S_Φ	1.9368	0.6125	0.1937
$F_\Phi - 3$	3.9789	0.3979	0.0398

The moments are also found numerical from the velocity signals, and are given in table 6. Comparing these to the analytic values, and see that for $K = 10^3$, the skewness are a slightly higher for degenerated distributed position and slightly lower for the unifromly distributed positions, compared to the analytic values. The excess kurtosis for the same case are nearly double for both the degenerated distributed position and uniformly distributed position. For higher K, the values are more equal to the theoretical values. When $K = 10^4$ there are still a slightly difference for the skewness value for both the cases. For the excess kurtosis, when the position are degenerated distributed, the values are more similar than for the uniformly distributed positions where the value are higher than the theoretical. For the last case with $K = 10^5$, the both the skewness and excess kurtosis are similar when the position is degenerated distributed. When the position is uniformly distributed, the differences are higher for this case.

Table 6: The skewness, S_Φ and excess kurtosis $F_\Phi - 3$ for the different cases, found numerically from the simulated signals.

amp = 1	K = 10^3	K = 10^4	K = 10^5
S_Φ	2.3667	0.5845	0.1829
$F_\Phi - 3$	6.4484	0.4407	0.0289
amp = 1, posy	K = 10^3	K = 10^4	K = 10^5
S_Φ	1.8327	0.6753	0.2254
$F_\Phi - 3$	6.0488	0.6814	−0.0245

6.2.1 Probability density function, PDF

In this section the probability density function, is presented in figure 21, for the different cases shown above. Start by looking at the plot with amplitude set to be constant. For the case with $K = 10^3$, the same shape is shown, as for the ion saturation current signal, where the singular pulses is first represented. In this case the single pulses is shown up to around $\widetilde{U}_{ExB} \approx 2$, which corresponds with what's shown in the For the other two cases where $K = 10^4$ and $K = 10^5$, the PDF's are quite similar, but there are more negative values for $K = 10^5$. Looking at the estimated intermittency parameters, γ, for the different cases, there are some differences. For $K = 10^3$ the intermittency parameter is given by $\gamma = 0.0942$, which is nearly what's assumed. However, looking at the curve-fit function, it only takes the PDF for the values after the singular pulses in the interval $[3, 5]$, which means that the whole time series is not well represented with the FPP-model. For $K = 10^4$ the estimated intermittency parameter is $\gamma = 12.8844$, which is not whats expected. The expected value in this case is $\gamma = 1$. Lastly, for $K = 10^5$, the intermittency parameter is $\gamma = 138.2532$, which is more than ten times the expected value.

In the plot representing the cases with uniformly distributed positions, in figure 21b, it looks quite similar to the other. The biggest difference is in the case with $K = 10^3$, where this one also presents negative values. This corresponds well with the time series in figure 20b, where there also

are negative values. In the same case, the singular pulses are well represented up to $\widetilde{U}_{ExB} \approx 4$, which also corresponds with the time series. Further, there are no big differences in the functions, compared to the previous case with degenerated distributed position. However, the intermittency parameter's are different. For $K = 10^3$, it is $\gamma = 0.0659$, which is lower than expected. Due to the bad curve-fit, the same as the previous discussion, it does not represent the whole time series good. For $K = 10^4$ the intermittency parameter $\gamma = 7.8489$ is closer to the expected value, but still not close enough. Lastly, for $K = 10^5$, $\gamma = 66.3945$, is also not nearly what's expected for this case.

For both the cases with degenerated distributed position and uniformly distributed positions, the PDF are not presenting the time series as expected, compared to the ion saturation current signal.

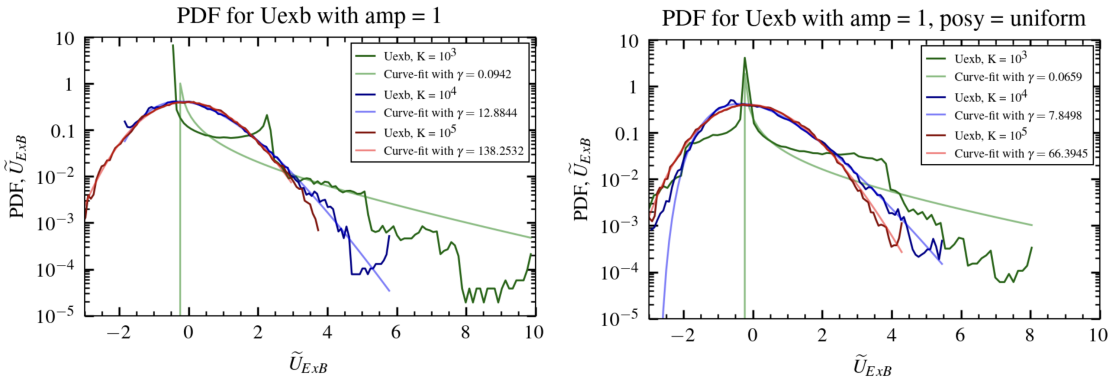

(a) (b)

Figure 21: The probability density functions for the velocity signal with different intermittency parameters.

6.2.2 Power spectral density, PSD

By using the FPP-model, the power spectral density (PSD) can also be presented. The PSD function describes the amount of energy for the different frequencies measured in the signal. In figure 22, the PSD function for the velocity signals, with amplitude set to one, is presented. From both functions in the figure, it comes clear that, also for the velocity functions, there are no variations due to the different number of blobs, expect for $K = 10^3$ when position is degenerated distributed. This is not expected, and may be a mistake in the time series, but this is unknown for now. The PSD functions are equal as long as the amplitude is set to one, which means that it does not depend on number of blobs K, or what the position in y-direction is set to.

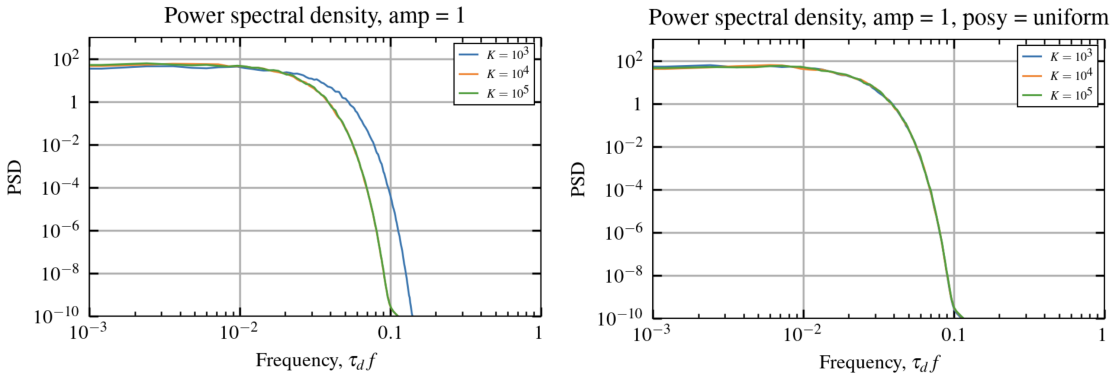

(a) (b)

Figure 22: The power spectral density for the velocity with amplitude set to one.

6.2.3 Conditional averaging

When using conditional averaging in the analysis, it will be interesting to look at two different cases. Firstly the signals can be analyses using the conditional averaging. Second, the signals can be analysed with conditional averaging, but using the ion saturation current (J_{sat}) as a reference signal. This way it is easier to see what happens with the velocity signal at the same time as the density signal. This is beneficial since the analysis for the density signal is already known. In this analysis, the lower threshold is set to 2.5, which means that the single pulses are avoided. This is easy to see for the first case with $K = 10$ and degenerated distributed position, that all the single pulses have amplitude lower than 2.5. It is important to have this in mind, when analysing the conditional averaging.

In figure 23a, the average pulse shape for the fluctuations in the time series is presented. Further, in figure 24, the same analysis as in 23, but with reference signal set to the density signal. See that there is a difference in the signal with different number of blobs. For $K = 10^3$, the duration time for this case are shorter than the two other cases. This corresponds well with the spectrum for the same cases in figure 22. For the other cases with $K = 10^4$ and $K = 10^5$, the pulse shape are similar. The same for the plots with uniformly distributed positions, where all the different cases has the same pulse shape. Where the average pulse shapes are similar, corresponds well with the PSD functions in figure 22.

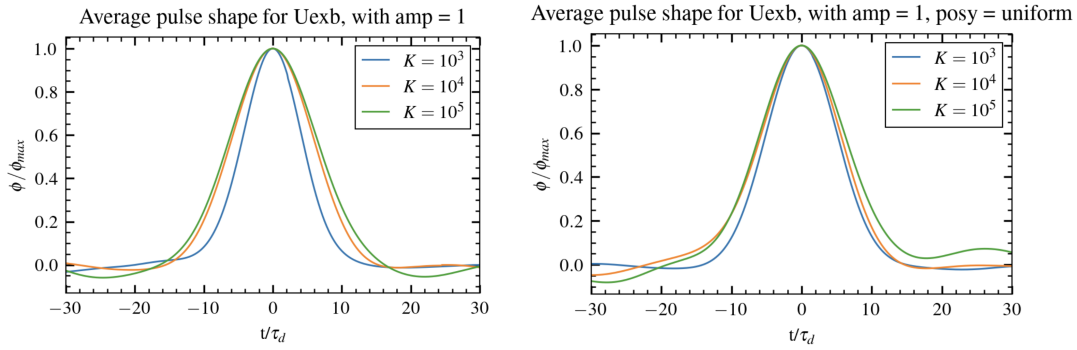

(a) (b)

Figure 23: The average pulse shape from conditional average for the different time series, with amplitude equal to 1.

In figure 24, the average pulse shapes are presented, compared to the ion saturation current, which is used as a reference signal. From the plots, both with degenerated distributed position, and uniform distributed position, the cases with $K = 10^4$ and $K = 10^5$ are the velocity pulse shapes after the J_{sat} pulses.

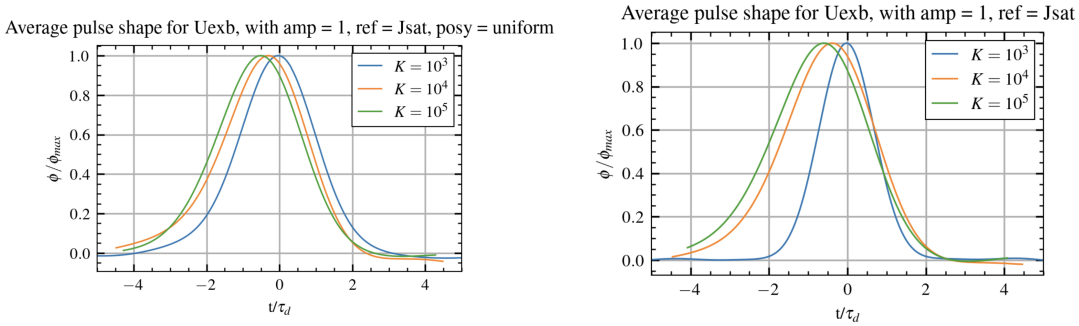

(a) (b)

Figure 24: The average pulse shape from conditional average for the different time series, with amplitude equal to 1. The conditional averaging has the ion saturation (J_{sat}) current as reference signal.

It is also necessarily to analyse the probability density function (PDF) for the conditional average waiting time for both the velocity signal and the velocity signal with density as reference signal. First, in figure 25, the waiting time distribution is presented. For the cases with degenerated distributed position in y-direction, they are similar to each other. All three cases have some spread, compared to the estimated curve-fit. Which means that the waiting time distributions is not perfectly fitted with an exponentially distributed fit-function. Moving on at the waiting time estimates, which are higher than expected. The reason for the high waiting times, is due to the high lower threshold, which eliminates many of the smaller pulses, and therefor affect the waiting time between pulses. The same is for the cases with uniformly distributed position. There are some larger differences between $K = 10^3$ and the other two cases. The estimated waiting times are also much higher than anticipated. However, for $K = 10^3$, the waiting time are significantly lower than for all the other cases. Looking back at the time series in figure 20b, there are more singular pulses included than for the other cases, which also gives a lower waiting time between the pulses.

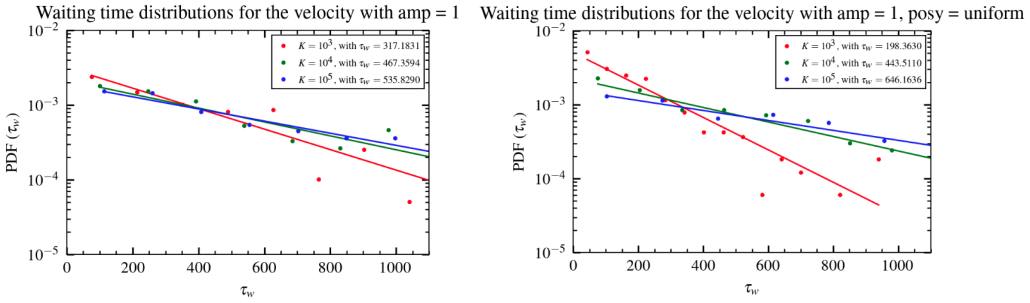

(a) (b)

Figure 25: The plot for the waiting time distribution. The plot shows waiting time distribution for the time series with amplitude equal to one.

Moving on to look at the same analysis as above, but with Jsat as a reference signal. The different waiting time distributions are spread in these plots as well. But the different cases are more equal each other. When looking at this analysis with J_{sat} as reference signal, the analysis are done based on the peaks in the reference signal. Which means that the waiting time distribution in figure 26, are the waiting times compared with the peak values for the reference. Compare the estimated waiting time values. For $K = 10^3$, the values are similar, but the second plot gives slightly higher estimated value. When $K = 10^4$, the estimated waiting time is nearly equal, and for $K = 10^5$ there are nearly the same difference than for the first case.

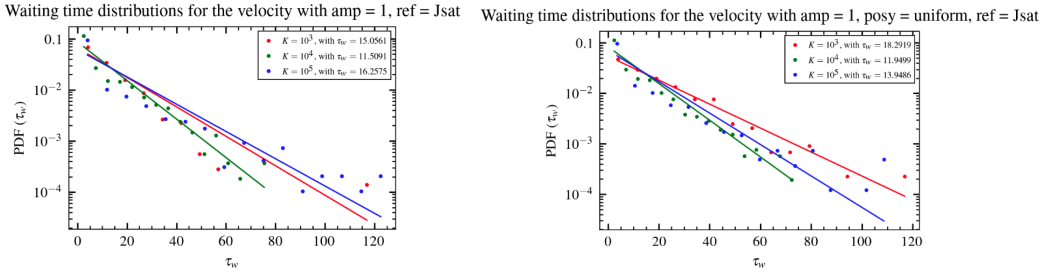

(a) (b)

Figure 26: The plot for the waiting time for the pulses. The plot shows waiting time for the time series with amplitude equal to one. The reference signal here is (J_{sat}).

The amplitude distributions are presented in figure 27. See that for $K = 10^3$, the different amplitudes are spread and the curve-fit are not a good representation for the distribution. For the other two cases, the curve-fit represents the amplitude distributions better.

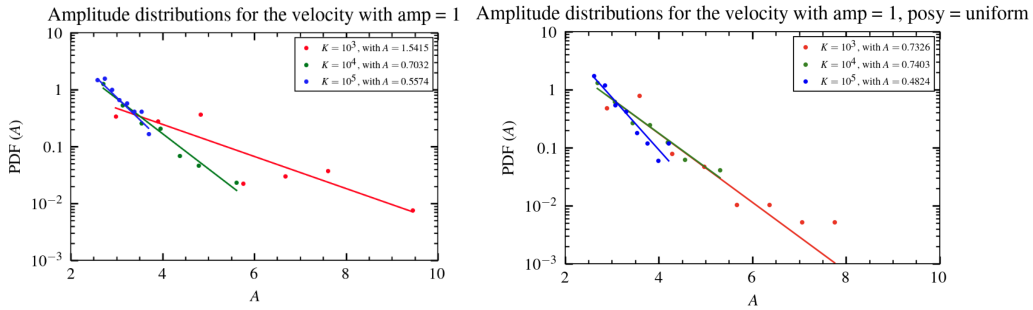

(a) (b)

Figure 27: The plot for the amplitude distribution. The plot shows amplitude distribution for the time series with amplitude equal to one.

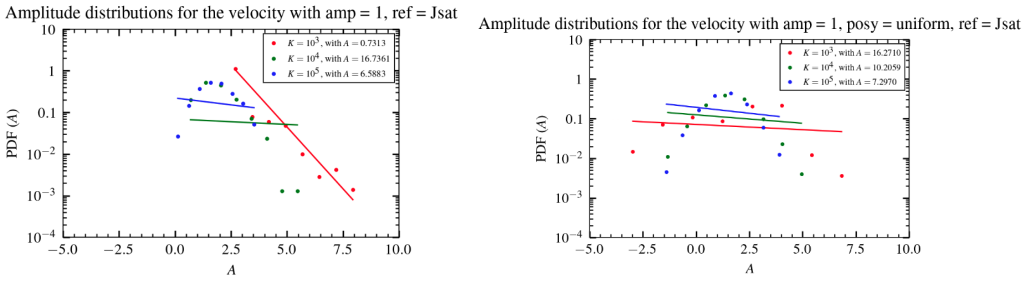

(a) (b)

Figure 28: The plot for the amplitude distribution. The plot shows amplitude distribution for the time series with amplitude equal to one. The reference signal used here is the ion saturation current (J_{sat}).

6.2.4 Summary of finds in analysing the velocity signal with amplitude set to one

In this section the main focus has been to investigate the velocity signals with amplitudes set to one. Started by looking at the time series and analysing skewness and excess kurtosis. In the time series it appears that the values for the signal are both positive and negative for the cases with uniformly distributed positions in y-direction. In the comparison between theoretical and numerical skewness and excess curtosis, it was discovered that both values are similar for almost all the cases.

In the FPP-analysis, the PDF's shown no good estimates for $K = 10^3$ with low degree of overlap, but are better for the two other cases. When looking at the estimated intermittency parameters for all the cases, no case has ha value near the expected values for the cases. This means that the PDF's does not fit the velocity signal good, especially when estimating the intermittency parameters. Further, in the PSD functions, there was an unexpected result in the case with $K = 10^3$ and amplitude set to one. It is expected that the PSD functions are independent of the number of blobs, K, and this may be a simulation mistake. During the conditional averaging analysis, the same results is shown in the average pulse shape, where this specific case has a lover duration time than the other pulses. Looking at the average pulse shape with J_{sat} as reference signals shows a small shift to the left for higher degree of overlap. For the waiting time distributions, it shows that the exponential distributed curve-fit is not a perfect fit for these distributions. The same goes for the amplitude distribution, but for the distribution with J_{sat} as reference signal, there are no exponentially distributed fit.

Based on the results for the velocity signal, the models does not represent the velocity signal as good as the ion saturation signal.

6.3 Results of the velocity signal with exponential distributed amplitude

The plots with exponentially distributed amplitudes, is given in figure 29. The plots show more variation in the velocity compared to when amplitude is set to one. For the cases with $K = 10^3$, the singular pulses are not so similar to each other compared to the previous cases. However, the cases are similar to the previous one, with amplitude set to one, where the degenerated distributed y-position gives positive values, and the uniform distributed y-positions gives both positive and negative values. Further in the cases for $K = 10^4$ and $K = 10^5$, is harder to see the singular pulses due to higher degree of overlap.

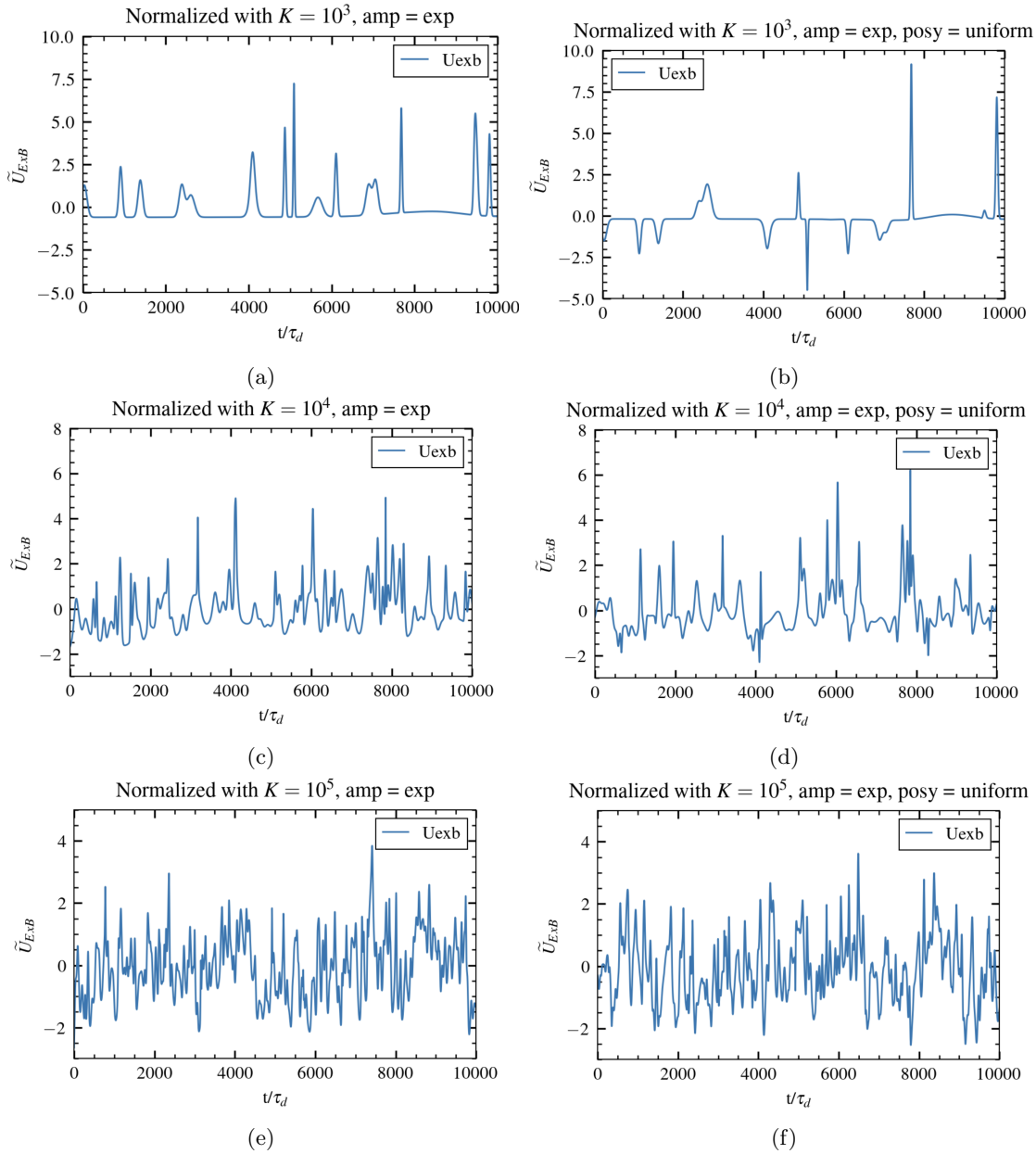

Figure 29: Plots of velocities for different number of blobs who are equally distributed blobs with amplitude as an exponentially distributed value. To the left the position in y-direction is set to be degenerated distributed, and to the right the position in y-direction is uniformly distributed.

Moving on to look at the skewness and kurtosis for the normalized signals. The theoretical values are given in table 7, and are the same values as presented in section 6.2, for amplitude set to one.

Table 7: The skewness, S_Φ and excess kurtosis $F_\Phi - 3$ for the different cases, calculated analytic.

Uexb, amp = 1	K = 10^3	K = 10^4	K = 10^5
S_Φ	1.9368	0.6125	0.1937
$F_\Phi - 3$	3.9789	0.3979	0.0398

In table 8, the numerically calculated values for the same moments are presented. Comparing the analytic results with the numerical results, and see that all the numerical values are higher than the analytic once. This indicates that the analytic calculations with amplitude set to one, does not represent the skewness and kurtosis for the exponentially distributed values. For the skewness values found numerically, there are only small differences due to the change of position distribution. This indicates that the changes for position in y-direction does not affect the symmetry of the signals. However, for the excess kurtosis, the values is almost doubled when setting position in y-direction to be uniformly distributed. These differnses apply for all the different cases, $K = 10^3, 10^4, 10^5$.

Table 8: The skewness, S_Φ and excess kurtosis $F_\Phi - 3$ for the different cases, found numerically from the simulated signals.

amp = exp	K = 10^3	K = 10^4	K = 10^5
S_Φ	4.0069	1.2359	0.4087
$F_\Phi - 3$	25.5578	2.5892	0.2824
amp = exp, posy	K = 10^3	K = 10^4	K = 10^5
S_Φ	4.3121	1.4098	0.4388
$F_\Phi - 3$	44.3451	4.9120	0.4769

6.3.1 Probability density function, PDF

The probability density functions for the time series, with exponentially distributed amplitude is presented in figure 30. The expected shape is a gamma distributed function, which is similar to both the green and the orange curve in figure 30, which represents the cases $K = 10^4$ and $K = 10^5$. This mean that the FPP-model fits better when the amplitude is set to be exponentially distributed. For $K = 10^3$, there is a clear difference compared to the case with amplitude set to one. The singular pulses are not presented as well as for the case with amplitude equal to one, in figure 21. There are also no clear difference due to the different distributions for the position in y-direction, expect for $K = 10^3$, where the values are all positive for degenerated distribution, and both positive and negative for uniformly distribution. This corresponds well with the time series for these signals given in figure 29a and 29b, and was also discovered for the same cases with amplitude set to one.

Further, looking at the estimated intermittency parameters, γ, for the different cases, which also can indicate the representation of the model. For $K = 10^3$, there are small differences in figure 30a, $\gamma = 0.4086$ and in figure 30b, $\gamma = 0.2339$. Even tough the intermittency parameters are similar to each other, they are further away from the expected value, $\gamma = 0.1$. The same applies to the other cases, where there are some small differences due to the positions in y-directions, but grater differences to the expected values. For $K = 10^4$, the estimated intermittency parameter are $\gamma = 3.0014$ and $\gamma = 2.3573$, and the expected value is $\gamma = 1$. Lastly, for $K = 10^5$ the $\gamma = 24.5996$ and $\gamma = 25.4179$ compared to the expected value $\gamma = 10$.

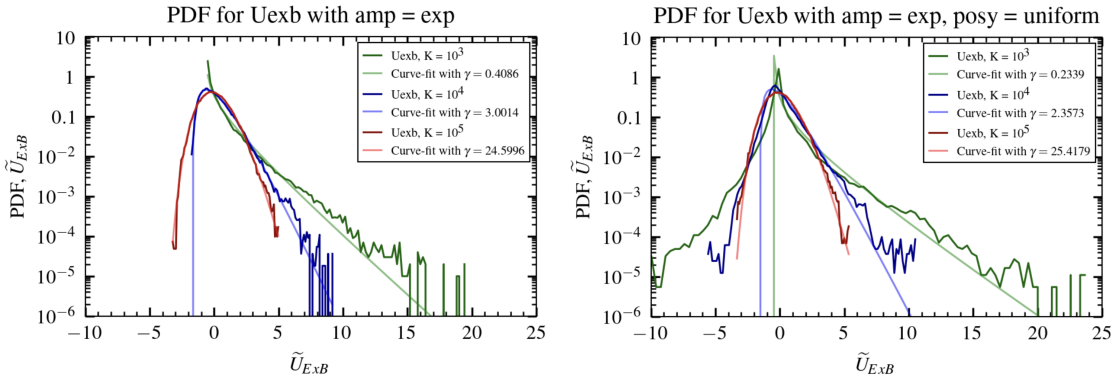

(a) (b)

Figure 30: Probability density function for the velocity signal with exponential distributed amplitude.

6.3.2 Power spectral density, PSD

The power spectral density for the velocity signal with exponentially distributed amplitudes. In figure 31, the PSD functions are presented for position in y-direction set to be degenerated distributed, and set to be uniformly distributed. The different cases gives similar PSD functions, which means that it is independent of both number of blobs K and the position in y-direction. Compared to the same plots for constant amplitudes, there are clear differences. By looking at the highest frequency, the exponentially distributed amplitudes gives ten times higher values than for the constant amplitudes.

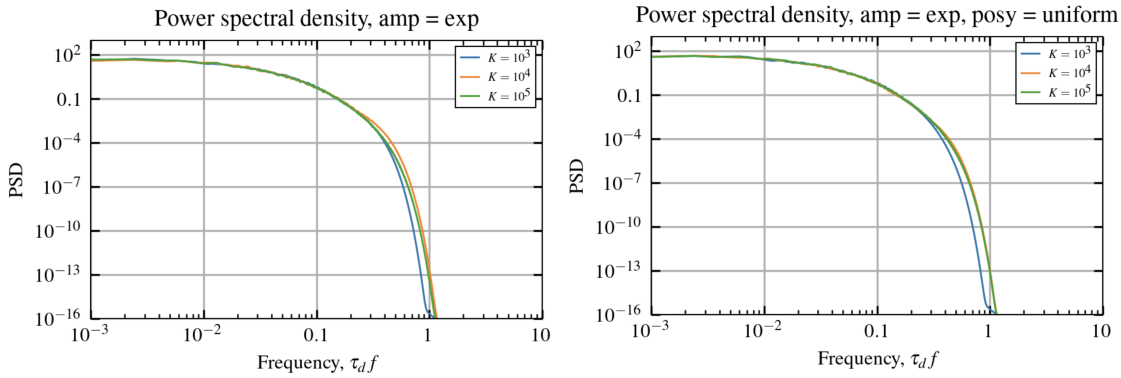

(a) (b)

Figure 31: Power spectral density for velocity signal with exponentially distributed amplitude.

6.3.3 Conditional averaging

The average pulse shape is for the velocity signal with exponentially distributed amplitude is presented in figure 32 and 33. Control, also in this cases, which values that are included with the lower threshold set to 2.5. For $K = 10^3$, the smallest pulses are avoided with this threshold. Same hold for both $K = 10^4$ and $K = 10^5$, only in these case it looks like fewer of the pulses are included in the conditional averaging.

Start by looking at the average pulse shapes, presented in figure 32. For all the different cases in the two plots, the pulse shapes, look similar with similar raise and decay time. The cases with $K = 10^3$ and $K = 10^4$, is most similar to each other, while $K = 10^5$, has some larger differences compared to the other cases. For the first plot with degenerated distributed y-position, $K = 10^5$, has some slower rise and decay time, than the other cases. The same tendency is for the plot with uniform distributed positions in y-direction, where $K = 10^5$ have slightly longer rise and decay than the other cases. This may be due to the higher degree of overlap in the case with $K = 10^5$, which can affect the average pulse shape.

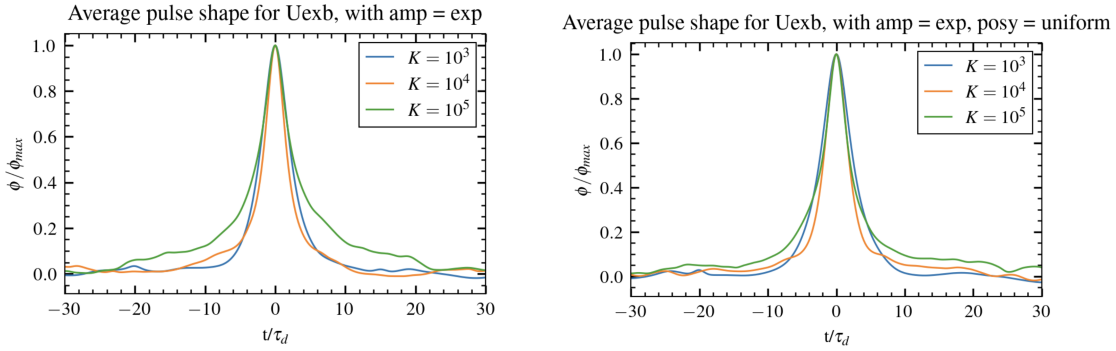

(a) (b)

Figure 32: The average pulse shape for velocity signal with exponentially distributed amplitude.

The same analysis is also shown with J_{sat} used as a reference signal. To be sure, the maximum value for all these average pulse shapes have been checked and are all equal to one. For the amplitude set to one, there were a clear shift in the average pulse shape for larger degree of overlap, $K = 10^4$ and $K = 10^5$. This is also shown in figure 33, with exponentially distributed amplitude. The shift is much smaller in this case, but still possible to see in the figures. Also in this plot the rise time are slower for $K = 10^5$, which also are due to the degree of overlap.

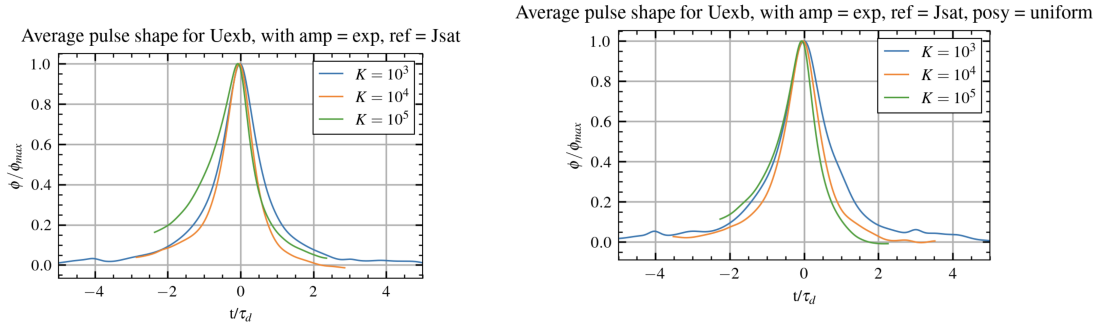

(a) (b)

Figure 33: The average pulse shape for velocity signal with exponentially distributed amplitude. The ion saturation current J_{sat} is set as reference signal.

By using conditional averaging, the waiting time distribution are presented in figure 34. Also in these cases the distribution of waiting times is not exponentially distributed, since the curve-fit does not fit as hope. For the plot with uniformly distributed position, in figure 34b, the exponentially distribution describes the waiting time better. The estimated waiting times presented in the plots are also higher than theoretical waiting time, which is a result of the lower threshold value.

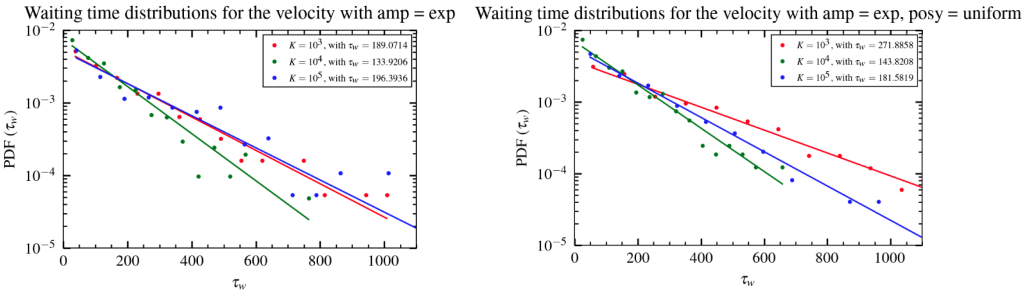

(a) (b)

Figure 34: The plot for the waiting time distribution. The plot shows waiting time distribution for the time series with exponentially distributed amplitude.

Now, looking at the waiting time distribution using the ion saturation current as a reference signal. These plots are presented in figure 35. These waiting time distributions described the waiting time for the velocity signal using peak values in J_{sat} as reference. The exponential distributed curve fit, gives a better estimate of the data points in this analysis. See that the case with $K = 10^3$ is quite different for the two other distributions, which is also whats shown in the same analysis for J_{sat}.

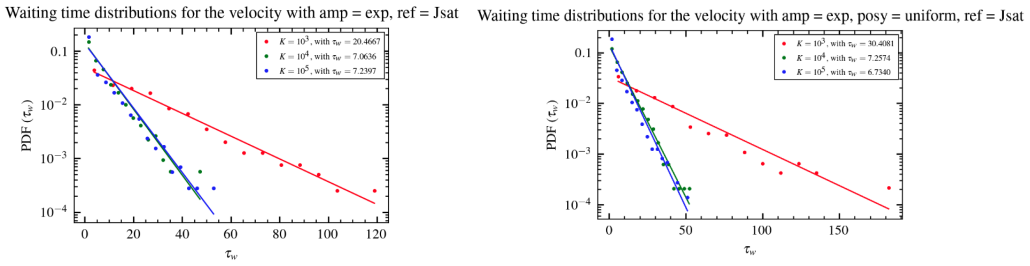

(a) (b)

Figure 35: The plot for the waiting time distribution. The plot shows waiting time distribution for the time series with exponentially distributed amplitude. The reference signal is J_{sat}

In figure 36, the amplitude distributions are presented. The exponentially distributed curve-fit, is nearly a good fit for these distributions. Compared to the previous discussion in section 6.2.3, with amplitudes set to one, these amplitudes are more correctly described by a exponentially distribution.

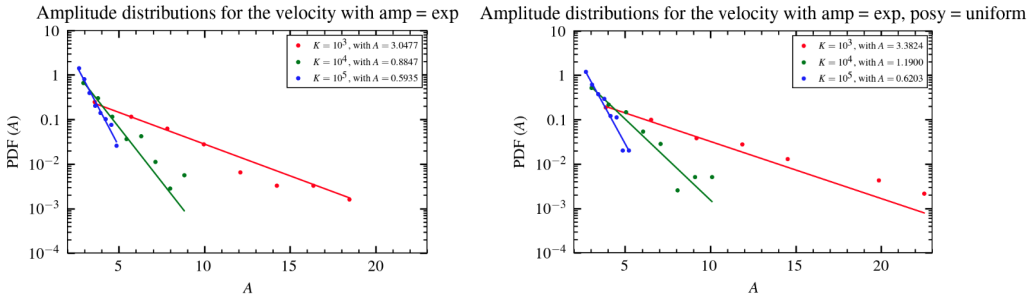

(a) (b)

Figure 36: The plot for the amplitude distribution. The plot shows waiting time distribution for the time series with exponentially distributed amplitude.

Lastly, looking at the amplitude distribution with J_{sat} used as the reference signal in figure 37. Only for $K = 10^3$ in the left plot are the amplitude distribution which is nearly a exponential distribution. The other distributions in both plots can't be described using the exponential distribution. From the plot, with logarithmic axes, the distributions show signs of a polynomial distribution.

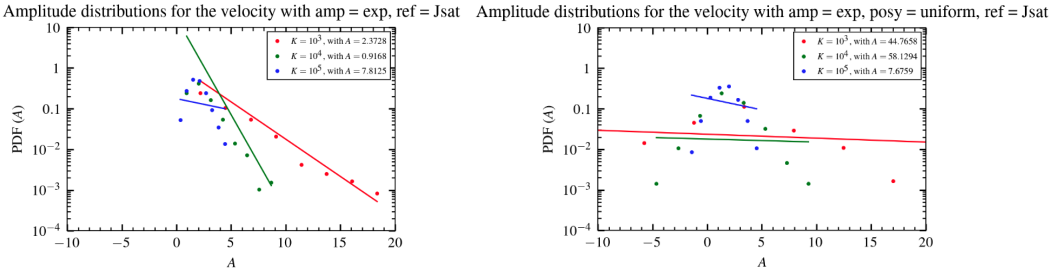

(a) (b)

Figure 37: The plot for the amplitude distribution. The plot shows waiting time distribution for the time series with exponentially distributed amplitude. The reference signal is J_{sat}.

6.3.4 Summary of finds in analysing the velocity signal with exponentially distributed amplitude

For this section, the cases with exponentially distributed amplitudes are presented and analysed. Also for these signals there are discovered both positive and negative values when the position in y-direction is uniformly distributed, which was expected based on the previous finds. When comparing the theoretical skewness and excess kurtosis for amplitude set to one with the numerical result for these time series, there are no similar values. Since there were no similarity for the same comparing with J_{sat}, it was not expected to see one in this analysis. Moving on to the PDF's which for higher degree of overlap, shows a good estimate for the functions. From the estimated intermittency parameter, it shows that the values are closer the expected values for these cases with exponentially distributed amplitudes. The PSD functions is as expected with no variations due to different K. In the conditional averaging, the average pulse shapes are as expected, and for the pulse shapes with J_{sat} as reference signal, there is also a slightly shift to the left. However, the shift was bigger for amplitudes set to one. When looking at the waiting time distributions, the exponential distributed curve fit is not a perfect estimate. For the waiting time distribution with reference in J_{sat}, the fit is surprisingly good, compared to the one with amplitudes set to one. The amplitude distributions shows the same as for amplitudes set to one, with some tendency of a good fit in the first plot, but for the plot, with reference signal, there are no good fit.

This mean that the FPP-model fits surprisingly good for the cases with exponentially distributed amplitudes, and the conditional averaging is as expected with deviations from the exponentially distributed curve-fit.

7 Conclusions and outlook

Using both the filtered Poisson process and conditional averaging to analyse different time series, has given much information about the capacity of the models. In this thesis there are chosen three different cases representing three different degree of overlap. These are separated using number of blobs, K, and set them to be $K = 10^3$, $K = 10^4$ and $K = 10^5$. This cases are simulated with two different amplitudes. First, for constant amplitudes set to one, and second, for exponentially distributed amplitudes. The cases has also had different distributions for the position in y-direction. First, the position has been degenerated distributed, and second, it has been uniformly distributed. All these cases are tested to see if the models has different outcome depended on the degree of overlap, K, the amplitude or the position distribution.

Started by analysing the ion saturation current, J_{sat}, using the FPP-model and conditional averaging. Analysed the signals first by looking at the skewness an the excess kurtosis, which showed similarity between the analytical values and the numerical values. The PDF showed good estimates for the higher degree of overlap. The models does not represent the signals with small degree of overlap, $K = 10^3$, which is known from analysis before. In the PSD functions, it is also confirmed that the signals are independent of number of blobs, and should also have constant duration time τ_d. In both the PDF and PSD functions, the difference, when changing the distribution of the position in y-direction, so small. This means that the model is representing the J_{sat}-signal good, independent of the distributions for the positions. The conditional averaging confirms the information's presented in the FPP-analysis, with the pulse shapes, waiting time distributions and amplitude distributions.

The velocity is analysed first for the cases with amplitude set to one. For the moments, there are some slightly similarity between the theoretical valued for skewness and excess kurtosis and the numerical values. For the case with $K = 10^3$, there are no good estimate in the PDF, but for the other two cases, the model gives a better fit. Moving on to the estimated intermittency parameters, there are no good estimates, and they are far from the theoretical inserted values. The PSD functions give a surprising result for $K = 10^3$, which shows that the PSD functions are dependent of K. This may be a mistake done in the simulations, and are not clarified at this point. This also shows in the average pulse shape, when using conditional averaging. For both the waiting time distribution and the amplitude distributions it shows that the exponential distributed curve-fit, may not present the cases well. For the amplitude distribution with J_{sat} as a reference signal, it looks like there are no good fit for the distribution, which clearly shows more of a polynomial shape.

In the analysis for the velocity signals with exponentially distributed amplitudes, the results are similar to the one above. But for the PDF's, it shows that for higher degree of overlap, there is a good estimate for the functions. From the estimated intermittency parameter, it shows that the values are closer the expected values for these cases with exponentially distributed amplitudes. The PSD functions are as expected, independent of K, which also gives a constant duration time, the same as for J_{sat}. This constant duration time τ_d is also shown in the average pulse shape, where the pulses for the different cases are similar. for the waiting time distribution and amplitude distributions the results are also similar to the other cases for velocity. Where the exponentially distributed curve-fit is not a good match for either the waiting time or the amplitude distributions.

Considering the results of the different analysis done in this thesis, it shows that parts of the hypothesis is correct. For the ion saturation current, the analysis fits well. It is also discovered that when changing the position distribution there are nearly no changes in the different function. This indicates that the model is a good fit and are robust enough to handle different changes, without letting i show in the analysis. For the velocity signals, the analysis show more doubtful results for some of the cases. The time series for the signals show also negative values for the velocity, which may cause some trouble in the analysis. However, there are some results which gives an indication that the FPP-model can be used for some of the velocity signals.

After analysing how the single-point measurements captures the ion saturation current and the velocity signals, it is safe to say the the J_{sat} is good represented for the analysing method and gives good results, when using the models. However, for the velocity signals, there are more various results, but some are showing good estimates. This means that the velocity signal may also be analysed using these model, but then including also the negative values in the signals.

A Code used in the analysis

The code used in this thesis can be found on: https://github.com/ema109/Master-

References

[1] Gregor. Blobmodel. https://github.com/uit-cosmo/blobmodel?tab=readme-ov-file, 2023.

[2] Eurofusion. https://euro-fusion.org/.

[3] O. E. Garcia. Blob transport in the plasma edge: a review. *Plasma and Fusion Research*, 4:019–019, 2009. doi:10.1585/pfr.4.019.

[4] E. Martinsen. Project paper, fys-3810 special curriculum. 2023.

[5] J. P. Freidberg. *Plasma Physics and Fusion Energy*. Cambridge University Press, 2007.

[6] A Theodorsen, O E Garcia, J Horacek, R Kube, and R A Pitts. Scrape-off layer turbulence in tcv: evidence in support of stochastic modelling. *Plasma Physics and Controlled Fusion*, 58(4):044006, jan 2016. URL: https://dx.doi.org/10.1088/0741-3335/58/4/044006, doi:10.1088/0741-3335/58/4/044006.

[7] R. Kube et al. Intermittent electron density and temperature fluctuations and assosiated fluxes in the alcator c-mod scrape-off layer. *Plasma Phys. Control. Fusion*, 2018.

[8] R. Kube and O. E. Garcia. Velocity scaling for filament motion in scrape-off layer plasmas. *Physics of Plasmas*, 18(10):102314, 10 2011. arXiv:https://pubs.aip.org/aip/pop/article-pdf/doi/10.1063/1.3647553/13610200/102314_1_online.pdf, doi:10.1063/1.3647553.

[9] R. Kube, O. E. Garcia, and M. Wiesenberger. Amplitude and size scaling for interchange motions of plasma filaments. *Physics of Plasmas*, 23(12):122302, 12 2016. arXiv:https://pubs.aip.org/aip/pop/article-pdf/doi/10.1063/1.4971220/16008027/122302_1_online.pdf, doi:10.1063/1.4971220.

[10] Kunnskapsdepartementet. Læreplan i fysikk (fys01-02). fastsatt som forskrift. læreplanverket for kunnskapsløftet 2020., 2021.

[11] A. Theodorsen. *Statistical properties of intermittent fluctuations in the boundary of fusion plasmas*. PhD thesis, UiT The Arctic Univercity of Norway, 2018.

[12] J. A. Bittencourt. *Fundamentals of Plasma Physics*. Springer, 2004.

[13] P C Stangeby. *The Plasma Boundary of Magnetic Fusion Devices*. Bristol; Philadelphia: Institute of Physics Pub, 2000.

[14] D. A. D'Ippolito, J. R. Myra, and S. J. Zweben. Convective transport by intermittent blob-filaments: Comparison of theory and experiment. *Physics of Plasmas*, 18(6):060501, 06 2011. arXiv:https://pubs.aip.org/aip/pop/article-pdf/doi/10.1063/1.3594609/13458678/060501_1_online.pdf, doi:10.1063/1.3594609.

[15] O. E. Garcia and A. Theodorsen. Auto-correlation function and frequency spectrum due to a super-position of uncorrelated exponential pulses. *Physics of Plasmas*, 24(3):032309, 03 2017. arXiv:https://pubs.aip.org/aip/pop/article-pdf/doi/10.1063/1.4978955/15936781/032309_1_online.pdf, doi:10.1063/1.4978955.

[16] O. E. Garcia, R. Kube, A. Theodorsen, and H. L. Pécseli. Stochastic modelling of intermittent fluctuations in the scrape-off layer: Correlations, distributions, level crossings, and moment estimation. *Physics of Plasmas*, 23(5):052308, 05 2016. arXiv:https://pubs.aip.org/aip/pop/article-pdf/doi/10.1063/1.4951016/15932366/052308_1_online.pdf, doi:10.1063/1.4951016.

[17] R. A. B. Nilsen. Conditional averaging of overlapping pulses, 2023.

[18] A Theodorsen and O E Garcia. Probability distribution functions for intermittent scrape-off layer plasma fluctuations. *Plasma Physics and Controlled Fusion*, 60(3):034006, jan 2018. URL: https://dx.doi.org/10.1088/1361-6587/aa9f9c, doi:10.1088/1361-6587/aa9f9c.